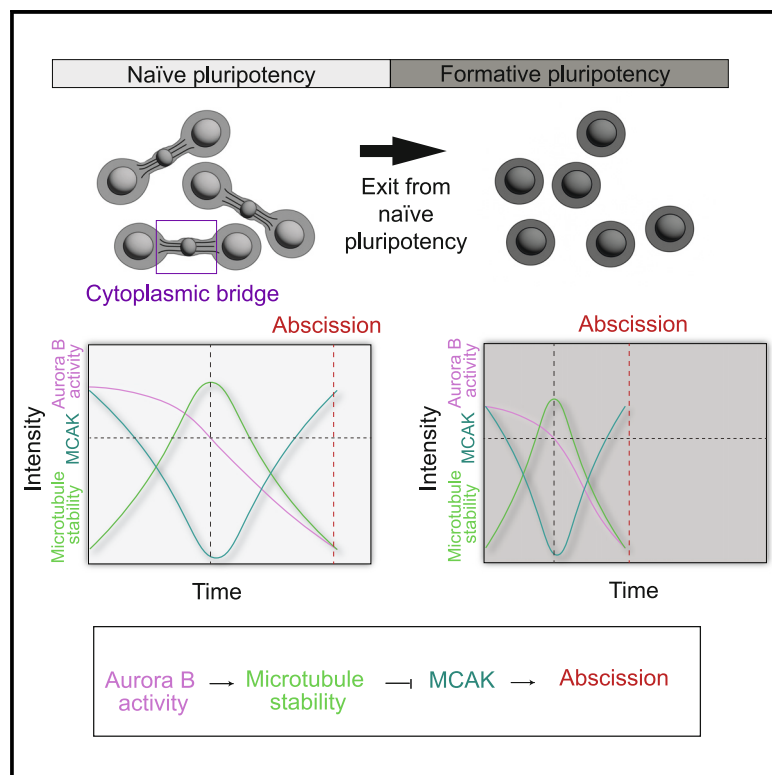


Aurora B controls microtubule stability to regulate abscission dynamics in stem cells

Graphical abstract



Authors

Snježana Kodba, Amber Öztop,
Eri van Berkum, ..., Wilco Nijenhuis,
Lukas C. Kapitein, Agathe Chaigne

Correspondence

a.e.d.chaigne@uu.nl

In brief

Mouse embryonic stem cells remain connected by bridges for hours after cell division. In this paper, Kodba et al. show that a high Aurora B activity at the bridge leads to microtubule stabilization. Stable microtubules recruit less of the microtubule depolymerase MCAK, which leads to bridge maintenance.

Highlights

- Aurora B controls abscission speed in mouse embryonic stem cells
- Aurora B activity leads to microtubule stabilization
- Microtubule stabilization prevents recruitment of MCAK and delays abscission



Article

Aurora B controls microtubule stability to regulate abscission dynamics in stem cells

Snježana Kodba,¹ Amber Öztop,¹ Eri van Berkum,¹ Eugene A. Katrukha,^{1,2} Malina K. Iwanski,¹ Wilco Nijenhuis,^{1,2} Lukas C. Kapitein,^{1,2} and Agathe Chaigne^{1,3,*}

¹Cell Biology, Neurobiology, and Biophysics, Department of Biology, Faculty of Science, Utrecht University, Padualaan, 3584 CS Utrecht, the Netherlands

²Centre for Living Technologies, Alliance TU/e, WUR, UU, UMC Utrecht, Princetonlaan 6, 3584 CB Utrecht, the Netherlands

³Lead contact

*Correspondence: a.e.d.chaigne@uu.nl

<https://doi.org/10.1016/j.celrep.2025.115238>

SUMMARY

Abscission is the last step of cell division. It separates the two sister cells and consists of cutting the cytoplasmic bridge. Abscission is mediated by the ESCRT membrane remodeling machinery, which also triggers the severing of a thick bundle of microtubules. Here, we show that rather than being passive actors in abscission, microtubules control abscission speed. Using mouse embryonic stem cells, which transition from slow to fast abscission during exit from naive pluripotency, we investigate the molecular mechanism for the regulation of abscission dynamics and identify crosstalk between Aurora B activity and microtubule stability. We demonstrate that naive stem cells maintain high Aurora B activity on the bridge after cytokinesis. This high Aurora B activity leads to transient microtubule stabilization that delays abscission by decreasing MCAK recruitment to the midbody. In turn, stable microtubules promote the activity of Aurora B. Overall, our data demonstrate that Aurora B-dependent microtubule stability controls abscission dynamics.

INTRODUCTION

Cell division is crucial to multicellular development and involves highly conserved protein complexes used to separate the chromosomes and the cytoplasm of one mother cell into two daughter cells. However, during mammalian development, cellular fate changes are associated with rapid and profound changes in the regulation of the cell division machinery. In particular, pluripotent stem cells remain connected with their sister cells through cytoplasmic bridges for a protracted amount of time, while stem cells that have exited naive pluripotency do not.¹ Instead, they rapidly sever this connection in a process called abscission. However, we do not know how abscission duration can be rapidly modulated to allow fate changes during development.

Abscission is a complex process whose building blocks are laid out at anaphase. At the center of the spindle, several protein complexes are recruited by the overlapping microtubules of the central spindle, including PRC1, which crosslinks antiparallel microtubules,^{2–4} centralspindlin which contains in particular the microtubule motor KIF23,⁵ and the chromosomal passenger complex (CPC).⁶ The CPC contains the kinase Aurora B, as well as INCENP, Borealin, and Survivin, and participates in the correct alignment of the chromosomes before anaphase is triggered. The central spindle signals to the cell cortex, which triggers the formation and constriction of an acto-myosin ring, leading to the formation of two cells connected by a cytoplasmic bridge. The cytoplasmic bridge contains microtubules and a dense structure called the midbody at the center of the bridge.

The midbody notably contains proteins from the central spindle, including the CPC, PRC1, and KIF23.^{7–9} The midbody then serves as a platform for the recruitment of a complex machinery that mediates the severing of the cytoplasmic bridge.¹⁰ Briefly, KIF23 recruits Cep55,¹¹ which in turn recruits Tsg101 and Alix.^{12,13} Tsg101 and Alix both interact directly or indirectly with members of the endosomal sorting complex required for transport (ESCRT) complex, leading to the formation of filaments of ESCRT-III.^{14–21} These filaments are remodeled by the AAA-ATPase VPS4²² and subsequently delocalize from the midbody to the midbody arms, which triggers the severing and resealing of the plasma membrane.^{15,23,24}

Importantly, the contents of the cytoplasmic bridge must be removed prior to ESCRT-III-mediated abscission.²⁵ Actin remodeling is critical for abscission completion.^{26–29} Microtubule removal is thought to be a passive event depending on membrane remodeling. Indeed, in parallel to ESCRT-III-mediated scission events, CHMP1B, a member of the ESCRT-III family, recruits the microtubule-severing protein spastin.^{30,31} Spastin then mediates microtubule severing and clearing from the cytoplasmic bridge.^{23,30–33} As such, microtubules are not thought to actively contribute to the timing of abscission, with their removal depending on the dynamics of ESCRT recruitment. Another microtubule severing protein, Katanin, can interact with the ESCRT-III binding domain microtubule interacting and trafficking (MIT)³⁴ and has been implicated in abscission.³⁵ Furthermore, recent data suggest that in cancer cells, microtubule severing happens much earlier than membrane severing and depends



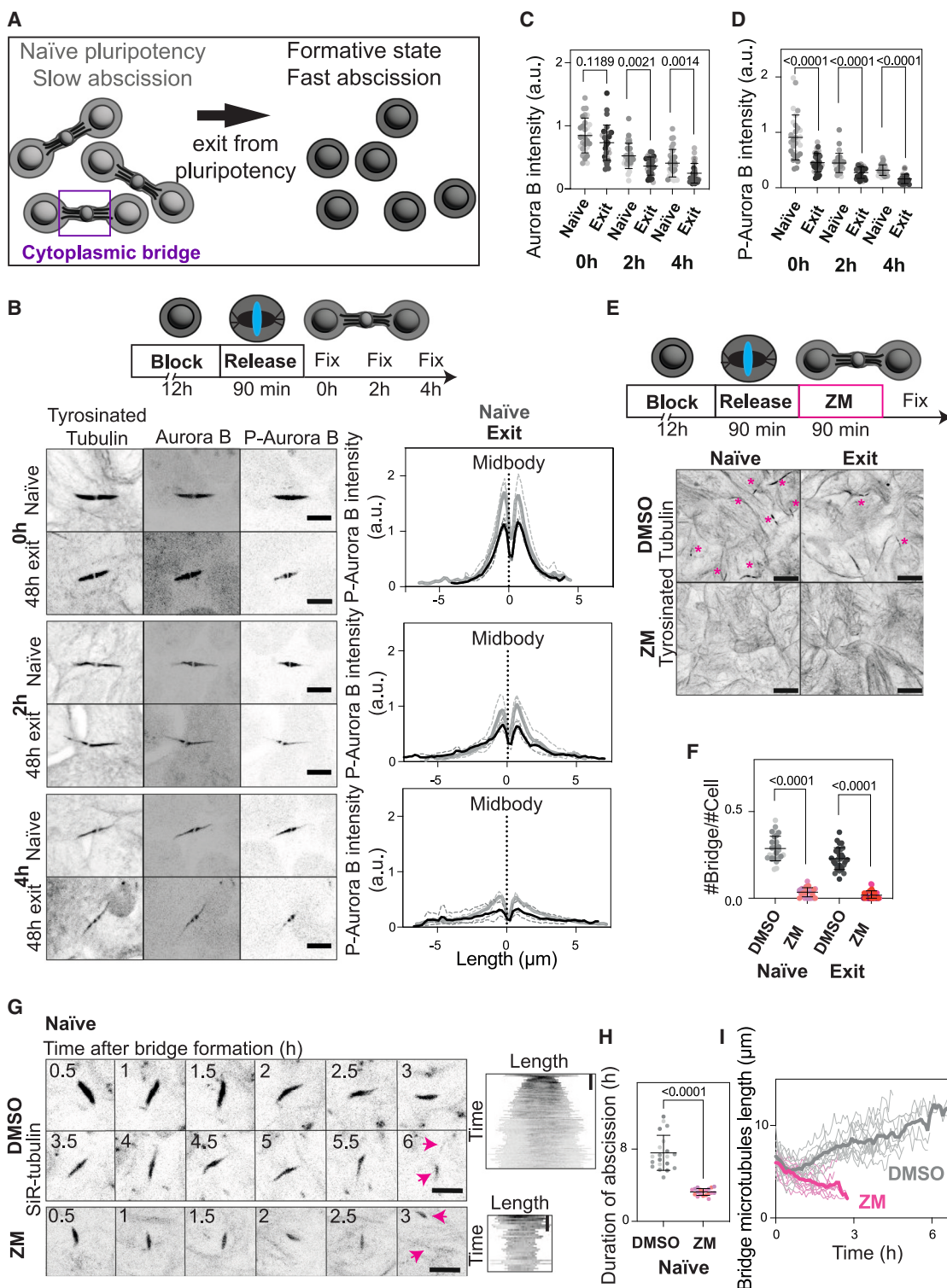


Figure 1. Aurora B activity controls abscission speed

(A) The dynamics of abscission during exit from naïve pluripotency in mouse embryonic stem cells (ESCs).

(B) Top: schematic of the experimental setup. Bottom left: immunofluorescence showing the localization of Aurora B and P-Aurora B in naïve and 48 h exiting ESCs during bridge maturation at bridge formation (0 h), 2 h after bridge formation (2h), and 4 h after bridge formation (4h). Scale bars: 5 μm . Bottom right: line scans showing the intensity of P-Aurora B along the length of bridges. The mean of $n = 10$ cells per replicate is plotted in dotted lines, and the mean of $N = 3$ replicates is plotted in solid lines.

(legend continued on next page)

on actin dynamics,²⁹ suggesting that multiple mechanisms could be at play in microtubule severing and abscission.

Abscission dynamics are mediated by the recruitment and re-positioning of ESCRT-III filaments from the midbody to the future abscission site on the midbody arms. In cancer cells, the CPC controls the proper localization of ESCRT-III filaments and therefore the timing of abscission. The CPC directly phosphorylates the ESCRT-III member CHMP4C,^{24,36,37} which leads to its retention at the midbody or in the cytoplasm and delays abscission. Aurora B activity also controls the localization of VPS4 at the abscission site.³⁸ The role of Aurora B in regulating abscission dynamics is not limited to cancer cells but is also important in the germ line³⁹ and in mouse embryos.⁴⁰ Interestingly, Aurora B can also regulate the microtubule cytoskeleton during abscission and, in particular, phosphorylates the microtubule motor KIF20A,⁴¹ which inhibits abscission. Surprisingly, spastin, which is important for severing microtubules and promoting abscission,^{30–32} has also been shown to be required for abscission arrest in cases of mitotic defects,³⁴ suggesting that microtubules could be a downstream target of Aurora B and an underestimated player in abscission dynamics. However, how microtubules regulate abscission dynamics is not known.

Here, we use mouse embryonic stem cells, which transition from slow to fast abscission during development, as a model system to investigate a direct role of Aurora B-dependent microtubule stability in controlling abscission. We show that in pluripotent cells, Aurora B activity is locally maintained at high levels at the exit of cell division. Aurora B activity regulates the duration of abscission in stem cells by controlling the stability of microtubules, with high Aurora B activity leading to an increased mass of stable microtubules. In turn, stable microtubules prevent abscission directly by preventing the recruitment of the depolymerase mitotic centromere-associated kinesin (MCAK), and indirectly by enhancing Aurora B activity. Finally, we show that Aurora B activity controls the dynamics of exit from naive pluripotency. Together, our results demonstrate that Aurora B can regulate abscission and cell fate by regulating microtubule stability.

RESULTS

Aurora B activity decreases slowly during bridge maturation in naive ESCs

To study the dynamics of abscission, we used mouse embryonic stem cells (ESCs) as a model system as they undergo a switch from a slow (6 h) to a fast (2–3 h) abscission when they exit naive pluripotency¹ (Figure 1A). Using naive cells (in 2i-Lif media, naive

ESCs) and exiting cells (48 h in N2B27 media, exiting ESCs) we can compare the same cell line undergoing either slow or fast abscission. Before abscission, cytoplasmic bridges are formed and matured, during which the diameter of the bridge narrows.^{1,23,26} To be able to compare bridges of the same age, we synchronized cells before mitotic entry using the CDK1 inhibitor RO-3306, then released the cells for 90 min (see STAR Methods). Cells were then fixed immediately (time point 0 h, which corresponds to bridge formation) or after 2 or 4 h.

Since Aurora B has been implicated in abscission regulation in multiple contexts, we first investigated its involvement in the abscission of ESCs. Aurora B was present over the length of the bridges of naive ESCs and exiting ESCs, in particular, in the area flanking the midbody (Figure 1B). The levels of Aurora B decreased over time in naive and exiting ESCs, with levels remaining overall higher in naive cells (Figures 1B and 1C). To test whether Aurora B activity was also higher in naive ESCs, we stained the cells with an antibody that specifically recognizes the phosphorylation of Thr232 of Aurora B.⁴² Similar to Aurora B, the levels of phosphorylated (P)-Aurora B decreased over time (Figures 1B and 1D). Strikingly, naive ESCs had higher levels of P-Aurora B than exiting ESCs at all time points of bridge maturation (Figures 1B and 1D). Finally, we wanted to test whether the higher activity of Aurora B at the bridge of exiting cells was linked to an overall higher activity of Aurora B in exit cells or specific to the bridge. To do so, we compared the levels of P-Aurora B in metaphase cells in naive and exiting cells and found that the levels were similar (Figures S1A and S1B). Thus, our data show that naive ESCs have higher levels of Aurora B activity than exiting ESCs specifically on cytoplasmic bridges and that this activity decreases during bridge maturation.

Aurora B regulates abscission dynamics in mouse ESCs

Next, we tested whether decreasing Aurora B activity impacts abscission duration. Because the CPC is involved in the spindle assembly checkpoint, to investigate the role of Aurora B in abscission, we again synchronized cells before mitotic entry using the CDK1 inhibitor RO-3306, then released the cells for 2 h before inhibiting Aurora B activity using ZM447439 (ZM hereafter). After 90 min of Aurora B inhibition, the localization and amount of Aurora B was unaffected in naive ESCs and slightly decreased in exiting ESCs (Figures S1C and S1E), whereas the activity of Aurora B was strongly reduced both in naive and exiting ESCs (Figures S1D and S1F). The number of bridges was strongly reduced in both naive and exiting ESCs treated with ZM (Figures 1E and 1F), suggesting that abscission is faster when Aurora B activity is abolished, in agreement with previous

(C) Quantification of Aurora B intensity in naive and exiting ESCs. Mean \pm SD. $N = 3$ replicates.

(D) Quantification of P-Aurora B intensity in naive and exiting ESCs. Mean \pm SD. $N = 3$ replicates.

(E) Top: schematic of the experimental setup. Bottom: immunofluorescence showing the number of bridges in naive and 48 h exiting ESCs treated with DMSO or 2 μ M ZM447439. Bridges: pink asterisks. Scale bars: 10 μ m.

(F) Quantification of the number of bridges per cell in naive ESCs treated with DMSO or 2 μ M ZM447439 and exiting ESCs treated with DMSO or 2 μ M ZM447439. $N = 3$ replicates.

(G) Live-cell imaging of naive ESC incubated overnight with 20 nM SiR-tubulin after the addition of DMSO or 2 μ M ZM447439. The pink arrows indicate the cut sites. One frame is shown every 30 min. Scale bars: 10 μ m. Right: kymographs showing the signal intensity over the length of the bridge over time. Scale bars: 1 h.

(H) Quantification of the duration of abscission from the bridge formation until microtubule severing in naive ESCs treated with DMSO or 2 μ M ZM447439. Mean \pm SD. $N = 3$ replicates.

(I) Quantification of the length of the bridge microtubule bundle in naive ESCs treated with DMSO or 2 μ M ZM447439 as a function of time.

work in other model systems.^{40,43} To confirm this, we imaged naive ESCs incubated with the live microtubule probe SiT-tubulin from anaphase onset to microtubule severing with or without ZM. We used the rupture of the microtubule bundle as a proxy for abscission, as membrane rupture always promptly follows the rupture of the microtubule bundle in our model system (Video 1; 3/10 cells cut the membrane less than 5 min after microtubule rupture and 7/10 cells cut the membrane between 5 and 10 min after microtubule rupture, $N = 3$ independent experiments). Control cells cut the cytoplasmic bridge in 7 h, while cells treated with ZM were twice as fast (Figures 1G and 1H; Videos 2 and 3). Abscission duration was also shorter in exit cells when treated with ZM (1 h ± 17 min, compared to 3.7 h ± 58 min in control cells). Importantly and contrary to controls, when treated with ZM, the bundle of microtubules in the bridge decreased in size over time (Figures 1G and 1I; Videos 2 and 3), suggesting microtubules could be under the control of Aurora B activity.

To confirm the role of Aurora B, we tested whether phosphatases could oppose the effect of Aurora B. To do so, we inhibited the protein phosphatases PP1 and PP2A using okadaic acid (OKA).⁴⁴ Naive ESCs treated with OKA had an Aurora B intensity at the bridge that was similar to that of controls; exiting ESCs treated with OKA had slightly higher Aurora B intensity than controls (Figures S1G and S1I). In all cases, treatment with OKA led to increased Aurora B activity at the bridge (Figures S1H and S1J). Treatment with OKA also led to an increase in bridge number in exiting ESCs (Figures S1K and S1L), suggesting that inhibiting PP1 and PP2A slows abscission. To confirm the role of phosphatases in abscission dynamics, we added OKA in naive and exiting ESCs just after bridge formation and found that treatment with OKA did increase the duration of abscission in naive and exiting ESCs (Figure S1M; Videos 4 and 5). To exclude off-target effects of ZM, we used a second inhibitor of Aurora B, barasertib, and confirmed that inhibiting Aurora B activity decreased the number of bridges (Figures S1N and S1O). Finally, we confirmed that synchronizing the cells with RO-3306 did not lead to mitotic delays (Figure S1P). In conclusion, our data show that higher Aurora B activity in pluripotent ESCs delays abscission.

Aurora B activity delays exit from naive pluripotency

Our data showed that Aurora B activity is higher in naive ESCs than in ESCs exiting naive pluripotency. Therefore, we wanted to test whether the activity of Aurora B controls exit from naive pluripotency. To do so, we performed clonogenicity assays to functionally test the dynamics of exit; briefly, cells were exited from naive pluripotency for 20 h, then replated at clonal density in pluripotency media (2i-Lif) (Figure 2A). Counting the colonies led to an estimate of the colony-forming capacity of the cells, providing a functional test of the dynamics of exit from pluripotency (a faster exit will lead to fewer colonies). To test the role of Aurora B activity, we allowed cells to exit from naive pluripotency for 15 h, then treated them with ZM for 90 min, and allowed them to exit for a further 3 h before replating (Figure 2A). This treatment did not affect cell proliferation (Figure S2A). When Aurora B activity was decreased by ZM treatment, fewer colonies formed compared to control (normalized to 1), showing

that exit from naive pluripotency was accelerated (Figure 2B). To confirm these results, we used flow cytometry to analyze the fluorescence of cells expressing the pluripotency marker Rex1-GFP^{1,45,46} after a similar pulse of ZM treatment and found that cells treated with ZM could be clearly sorted into high-Rex1 and low-Rex1 (Figure 2B). Altogether, our data show that inhibiting Aurora B activity leads to a faster exit from pluripotency.

Microtubules are transiently stabilized in slowly abscising cells

Aurora B inhibition led to shorter microtubule bridges and a faster abscission, suggesting a crosstalk between Aurora B, microtubules, and abscission. Furthermore, Aurora B can regulate microtubule dynamics,^{47,48} and microtubules need to be severed for abscission. We therefore hypothesized that differences in Aurora B activity between naive and exit cells could control abscission dynamics by regulating microtubules. To test this, we imaged microtubules in maturing bridges in naive and exiting cells. As expected, given that the bridge narrows over time,¹ microtubule intensity in the bridge decreased over time until abscission (Figures 3A and 3B; Video 2). Cells can maintain microtubules over time by stabilizing them.⁴⁹ To test whether microtubules are more stable in naive cells, we used markers for post-translational modifications that predominantly decorate stable or dynamic microtubules.⁴⁹ We stained naive and exiting ESCs at different stages of bridge maturation for total tubulin, acetylated tubulin (which marks stable microtubules), and tyrosinated tubulin (which marks dynamic microtubules). Bridges were very dense structures containing acetylated and tyrosinated tubulin (Figures 3C; S3A). However, while total tubulin and tyrosinated tubulin intensity decreased over time (Figures 3C, 3D, S3A, and S3B), acetylated tubulin intensity initially increased prior to decreasing (Figures 3C and 3D). This increase was much more pronounced in naive ESCs than in exiting ESCs. This suggests a previously undescribed stage of transient microtubule stabilization during bridge maturation, which is more pronounced in naive cells and correlates with slow abscission.

To confirm this finding, we used a recently developed marker (StableMARK) to visualize stable microtubules in live cells.⁵⁰ Using StableMARK, we confirmed that the intensity of stable microtubules increases and then decreases over time in naive and exiting ESCs (Figures 3E–3I, S3D, and S3E; Video 6). Of note, StableMARK expressing naive and exit cells displayed delayed abscission compared to non-expressing cells, consistent with previous findings that StableMARK can induce microtubule stabilization at high expression levels⁵⁰ (Figure 3F; 11.6 h ± 4.6 h for naive cells versus 5.5 h ± 1.4 h in exit cells [compare to Figure 1H]). Finally, we wondered whether this transient increase in stable microtubules at the bridge was a general feature of dividing cells. To test this, we imaged a previously established cell line stably expressing StableMARK⁵⁰ and found that contrary to ESCs, U2OS expressing low levels of StableMARK had stable microtubules at the point of contact between the bridge and the cell bodies of the daughter cells, but only a limited amount of stable microtubules could be detected at this time-scale around the midbody throughout bridge maturation (Figures S3E and S3F). Thus, the transient but extended

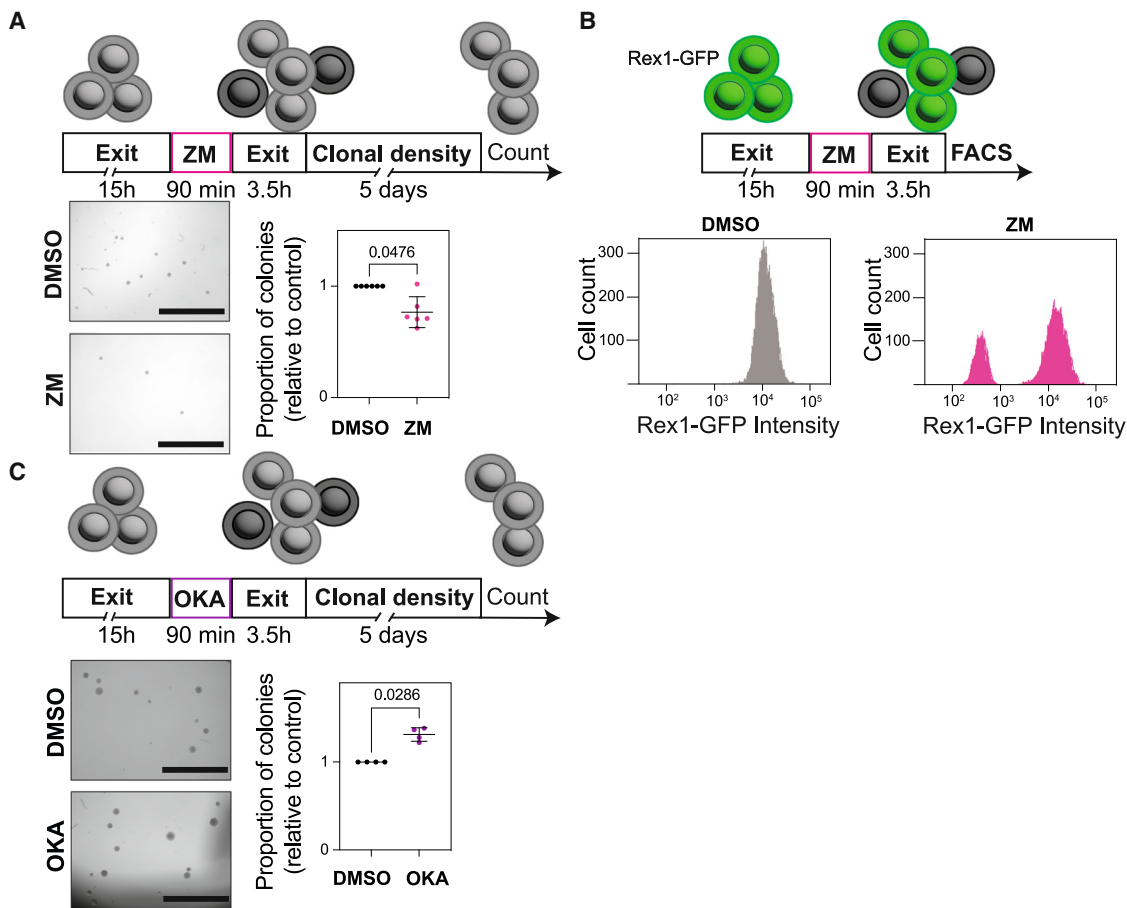


Figure 2. Aurora B activity controls exit from naive pluripotency

(A) Top: schematic of the experimental setup. Bottom: clonogenic assay on ESCs treated with 2 μ M ZM447439. Left: colonies formed by control cells after 20 h of exit from naive pluripotency and cells treated with ZM447439. Scale bars: 1 mm. Right: quantification of the number of colonies formed. Mean \pm SD. N = 6 replicates.

(B) Top: schematic of the experimental setup. Bottom: graphs showing the number of cells as a function of GFP intensity as measured by FACS in cells exiting naive pluripotency for 20 h treated with DMSO or ZM447439. One representative example is shown out of three experiments.

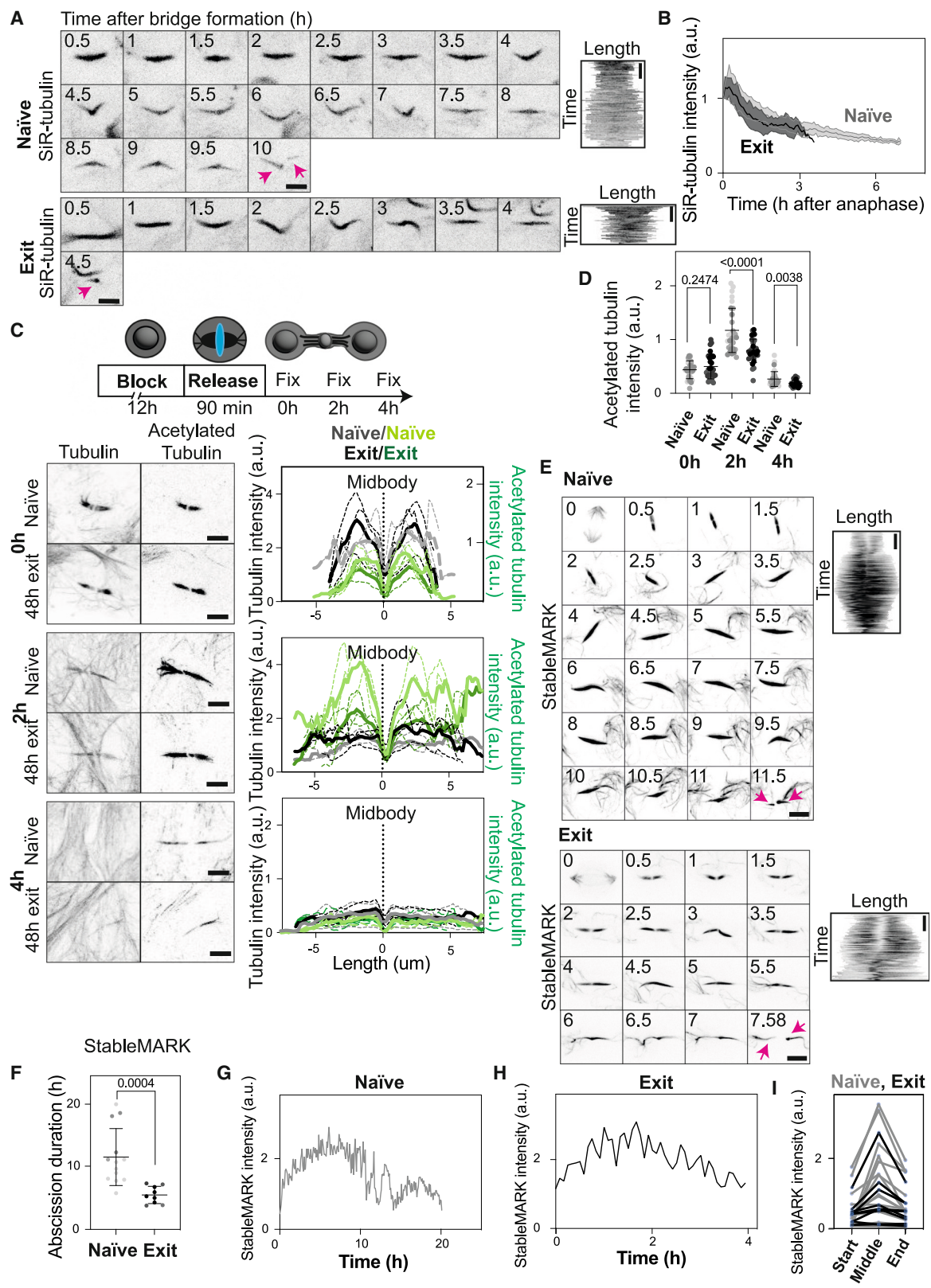
(C) Top: schematic of the experimental setup. Bottom: clonogenic assay on ESCs treated with 0.5 μ M okadaic acid (OKA). Left: colonies formed by control cells after 20 h of exit from naive pluripotency and cells treated with OKA. Scale bars: 1 mm. Right: quantification of the number of colonies formed. Mean \pm SD. N = 4 replicates.

stabilization of bridge microtubules along the length of the bridge could be a specific feature of stem cells.

Aurora B activity controls microtubule stability

We then wondered whether Aurora B could control microtubule abundance and stability. To test this, we inhibited Aurora B activity with ZM and stained for total tubulin. We first confirmed that bridges of cells treated with ZM were overall much shorter than control bridges (Figure 4A). Consistently, cells treated with ZM displayed less total tubulin, acetylated tubulin (Figures 4A–4D), and tyrosinated tubulin (Figure S4A–S4C), suggesting that inhibiting Aurora B activity decreases the number of microtubules. We then turned to live microscopy to test how the different populations of microtubules evolve over time. We analyzed the decrease in SiR-tubulin intensity (as a readout for all microtubules) in naive control cells and cells treated with ZM (Figures 1G and 1H; Video 2). We found that while the inten-

sity of SiR-tubulin was overall lower in ZM-treated cells compared to control (Figure S4D, bottom) consistent with our fixed data, when we normalized each curve with the first time point set as 1, the intensity of SiR-tubulin decreased over time with similar dynamics in ZM-treated naive cells and in controls (Figure S4D, top). Crucially, abscission always happened when microtubule intensity reached a similar threshold (Figure S4D, bottom). We then imaged specifically stable microtubules with StableMARK in naive ESCs and found that inhibiting Aurora B activity had a strong effect on stable microtubules, as the intensity of StableMARK decreased faster when cells were treated with ZM compared to controls (Figures 4E and 4F; Video 7). In particular, cells did not display the transient increase in stable microtubules described before (Figures 3F and 3H–3K). Altogether, our data indicate that high Aurora B activity leads to an increase in the abundance of microtubules, in particular, the stable population.



(legend on next page)

Microtubule stability controls abscission speed

Since Aurora B controls both microtubule stability and abscission speed, we hypothesized that microtubule stability could control abscission speed. To test the role of stable microtubules in abscission speed, we first stabilized microtubules using Taxol.

Stabilizing microtubules led to a small increase in Aurora B intensity (Figures S5A and S5B) and to a strong increase in P-Aurora B intensity (Figures 5A and 5B), suggesting that stabilizing microtubules leads to an overall increase in Aurora B activity. Stabilizing microtubules also led to an increase in the number of bridges (Figures 5C and 5D), suggesting that stabilizing microtubules slows abscission. To confirm this, we treated 48 h exiting ESCs expressing tubulin-GFP with Taxol and imaged cells during bridge maturation. While control cells divided normally, abscission was severely delayed or never happened in cells treated with Taxol (Figure S5C). These data suggest that microtubule stability prevents abscission. To confirm that microtubule stability, not microtubule amount, controls abscission speed, we treated cells with nocodazole, a drug that depolymerizes microtubules. Naive ESCs were treated with increasing doses of nocodazole. At low doses of nocodazole (0.5 and 1 μ M), the acetylated microtubules largely remained intact, while there was a decrease in tyrosinated microtubules (Figures S5D–S5G). At this concentration, the number of bridges was not affected (Figures 5E and 5F). At higher doses of nocodazole, we noticed a decrease in the amount of acetylated microtubules (Figures S5C–S5G), as well as a decrease in the number of bridges per cell (Figures 5E and 5F). Consistent with our data on Taxol-stabilized bridges, we also saw a decrease in the P-Aurora B amount only when the number of acetylated microtubules decreased (Figure S5G). Altogether, our data show that Aurora B activity on the bridge tracks stable microtubule levels and that stable microtubules prevent abscission.

To test the separate contributions of Aurora B and microtubule stability in regulating abscission, we treated cells simultaneously with ZM and Taxol after bridge formation. The two treatments combined led to a decrease in Aurora B activity (Figures S5H and S5I), a decrease in the intensity of acetylated tubulin (Figure S5J), and a decrease in the number of bridges per cell

(Figures S5K and S5L). These data indicate that microtubule stabilization does not rescue Aurora B inhibition, which confirms that Aurora B controls abscission through other downstream targets.

Finally, we compared the abscission dynamics of naive ESCs across our different conditions. While inhibiting Aurora B activity speeds up abscission, expressing StableMARK, which can lead to microtubule stabilization,⁵⁰ increased abscission duration; expressing StableMARK in cells with decreased Aurora B activity leads to a return to a slow abscission (Figure 5G). Collectively, our data show that the stability of microtubules and Aurora B activity control abscission dynamics.

Microtubule abscission occurs at zones of low stability

To confirm the causality of the relationship between low microtubule stability and abscission, we imaged StableMARK on both arms of the cytoplasmic bridges and compared the intensity between arms. We noticed that abscission happened asymmetrically, consistent with previous reports of asymmetric bridge remnants in stem cells (Video 1).⁵¹ Strikingly, shortly before and after abscission, the cut arm always displayed a lower intensity of StableMARK (Figures 6A–6D). These data show that lower levels of stable microtubules directly and locally correlate with abscission. We thus propose that in stem cells, high Aurora B activity leads to the stabilization of microtubules in the bridge, which prevents abscission. Locally, microtubules can be destabilized, which triggers asymmetric abscission on one arm only. To confirm this model, we fixed cells several hours after bridge formation (6 h after release in exiting ESC, 7 h after release in naive ESC) and investigated whether we could find an asymmetry in P-Aurora B and acetylated tubulin intensity in old bridges close to abscission. Strikingly, we found bridges that had asymmetric arms, with one arm showing a higher intensity of acetylated tubulin and P-Aurora B but no difference in tyrosinated tubulin intensity (Figure 6F). The asymmetry in the arms was found for 31.3% of naive cells and 33.8% of exit cells. This asymmetry was not obvious at earlier stages of bridge maturation (Figures 1B and 3C). Thus, our data suggest that close to abscission, the activity of Aurora B decreases locally and triggers a local decrease in microtubule stability, allowing for abscission.

Figure 3. Microtubules are stabilized during slow abscission

- (A) Live-cell imaging of naive and 48 h exiting ESCs incubated with 20 nM SiR-tubulin. One frame is shown every 30 min. The pink arrows indicate the cut sites (note that in the exiting example, only one arm remains in frame after cut). Scale bars: 5 μ m. Right: kymographs showing the signal intensity over the length of the bridge over time. Scale bars: 1 h.
- (B) Quantification of the intensity of SiR-tubulin over time. Mean \pm SD. N = 3 replicates.
- (C) Left: immunofluorescence showing the localization of total tubulin and acetylated tubulin in naive and 48 h exiting ESCs during bridge maturation at bridge formation (0 h), 2 h after bridge formation (2h), and 4 h after bridge formation (4h). Scale bars: 5 μ m. Right: line scans showing the intensity of acetylated tubulin along the length of bridges. The mean of n = 10 cells per replicate is plotted in dotted lines, and the mean of N = 3 replicates is plotted in solid lines. Total tubulin is shown in gray (naive cells in light gray, cells exiting pluripotency in dark gray) and acetylated tubulin is shown in green (naive cells in light green, cells exiting pluripotency in dark green).
- (D) Quantification of acetylated tubulin intensity in naive and exiting ESCs during bridge maturation. Mean \pm SD. N = 3 replicates.
- (E) Live-cell imaging of naive and 48 h exiting ESCs transfected with StableMARK. The pink arrows indicate the cut sites. One frame is shown every 30 min. Scale bars: 5 μ m. Right: kymographs showing the signal intensity over the length of the bridge over time. Scale bars: 1 h.
- (F) Graph showing the duration of abscission in naive or exiting ESCs expressing StableMARK. Mean \pm SD. N = 3 replicates.
- (G) Graph showing an example of the evolution of StableMARK intensity in a naive ESC over time. The rest of the analyzed cells are shown in Figure S3C.
- (H) Graph showing an example of the evolution of StableMARK intensity in a 48 h exiting ESC over time. The rest of the analyzed cells are shown in Figure S3D.
- (I) Graph showing the evolution of the intensity of StableMARK throughout bridge maturation in naive and 48 h exiting ESCs, using bridge formation as "Start," the last frame before bridge cutting as "End," and the frame halfway between these two points as "Middle." N = 5 replicates.

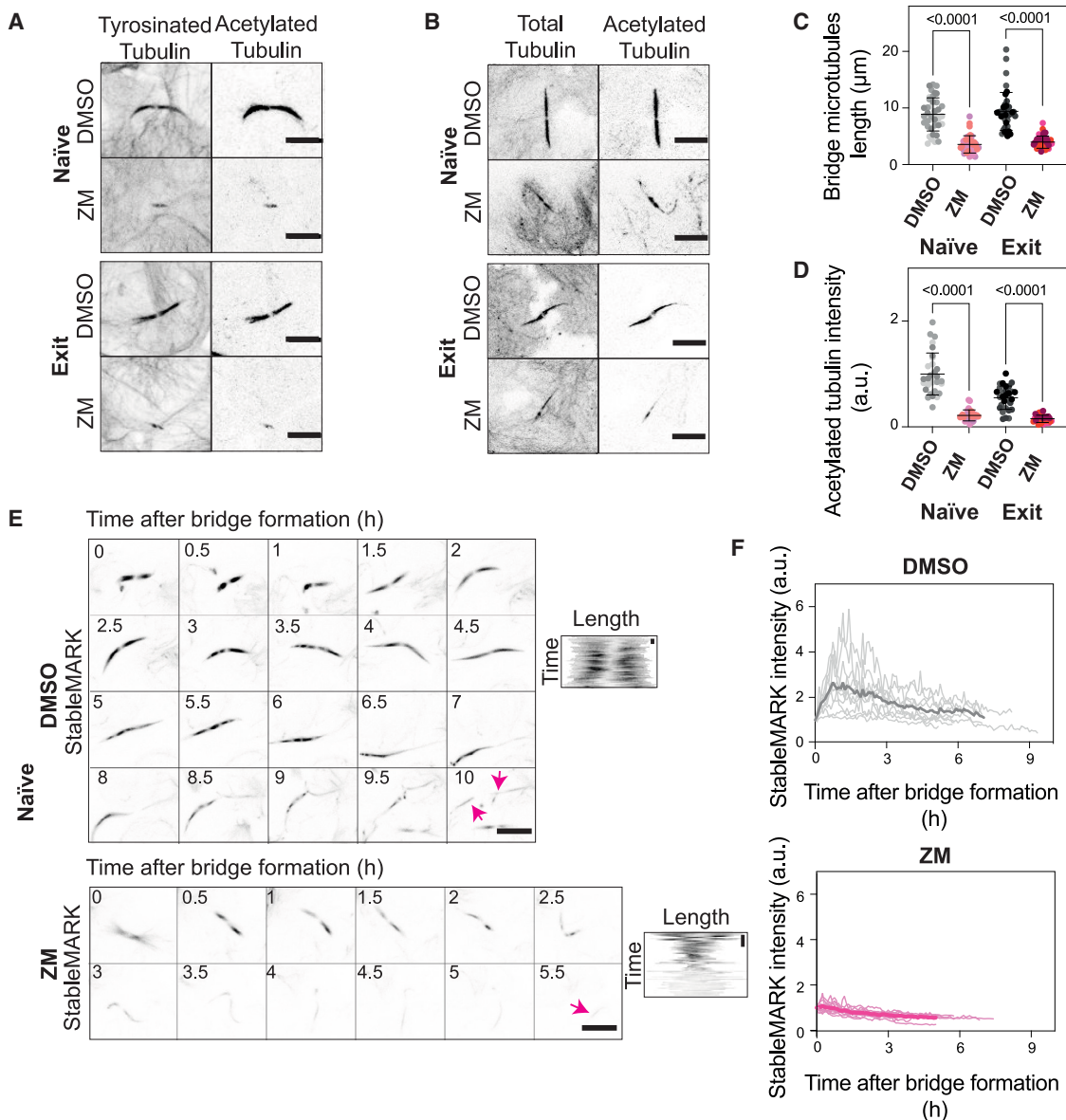


Figure 4. Aurora B activity controls microtubule stability

(A) Immunofluorescence showing the size of the bridges of naive or 48 h exiting ESCs treated with DMSO or 2 μM ZM447439. Bridges are stained for tyrosinated tubulin or acetylated tubulin. Scale bars: 5 μm.

(B) Immunofluorescence showing total tubulin and acetylated tubulin in naive or 48 h exiting bridges of ESCs treated with DMSO or 2 μM ZM447439. Scale bars: 5 μm.

(C) Quantification of the length of bridges in naive or 48 h exiting ESCs treated with DMSO or 2 μM ZM447439. Mean ± SD. N = 3 replicates.

(D) Quantification of the intensity of acetylated tubulin in naive or 48 h exiting ESCs treated with DMSO or 2 μM ZM447439. Mean ± SD. N = 3 replicates.

(E) Live-cell imaging of naive (top) and 48 h exiting (bottom) ESCs expressing StableMARK. The pink arrows indicate the cut sites (note that in the ZM-treated example, only one arm remains in frame after cut). One frame is shown every 30 min. Scale bars: 5 μm. Right: kymographs showing the signal intensity over the length of the bridge over time. Scale bars: 1 h.

(F) Quantification of the intensity of StableMARK over time in naive ESCs expressing StableMARK and treated with DMSO or 2 μM ZM447439. N = 3 replicates.

Microtubule stabilization prevents MCAK recruitment

Finally, we sought to understand how microtubule stabilization leads to a delay in abscission. We hypothesized that stable microtubules could be resistant to depolymerization by microtubule depolymerizing proteins. The plus-end microtubule depoly-

merase MCAK is an interesting candidate because it is located in the bridge in other cell types.⁴⁸ We found that in naive and exiting ESCs, MCAK localized to the bridge (Figure 7A). Importantly, during bridge maturation, MCAK intensity in the bridge decreased and then increased, particularly in naive cells

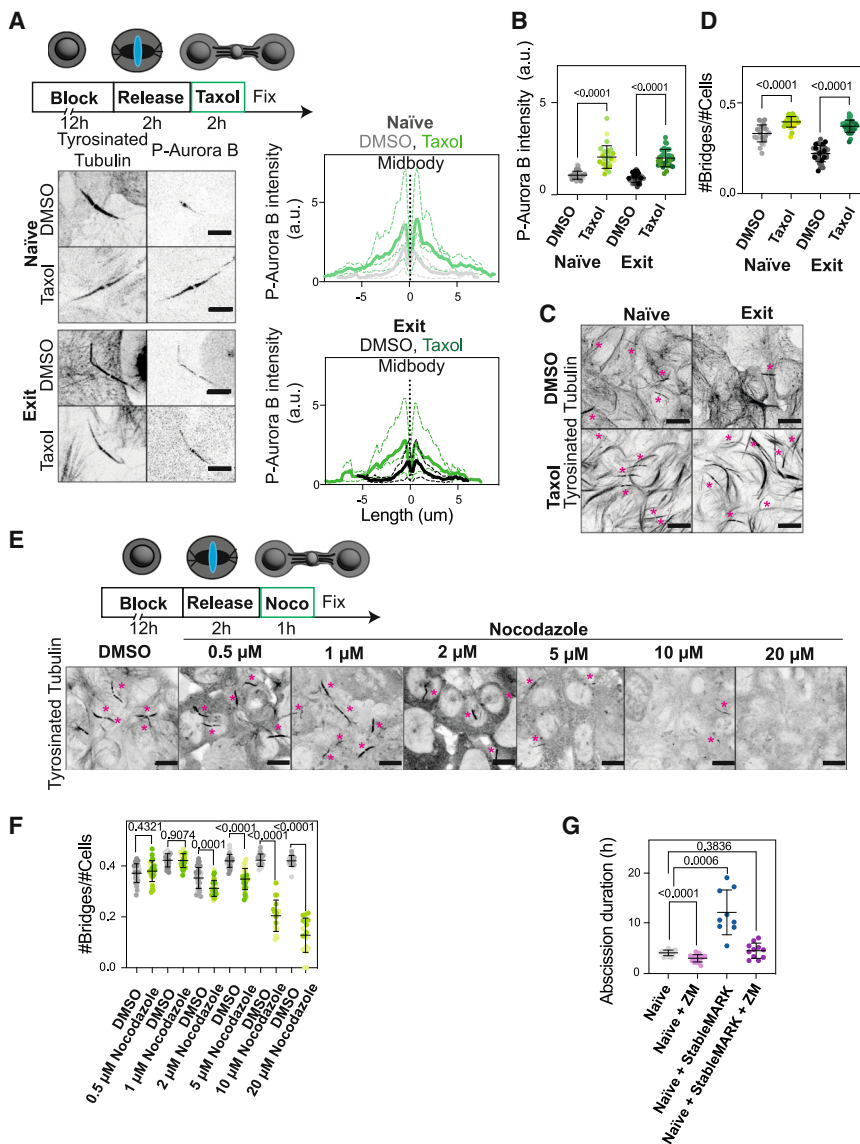


Figure 5. Increased microtubule stability delays abscission

(A) Left: immunofluorescence showing the localization of P-Aurora B in naive and 48 h exiting ESCs treated with DMSO or 0.5 μ M Taxol. The bridge is shown with the staining of tyrosinated tubulin. A Z-projection over the height of the whole cell is shown. Scale bars: 5 μ m. Right: line scans showing the intensity of P-Aurora B along the length of the bridges. The mean of $n = 10$ cells per replicate is plotted in dotted lines, and the mean of $N = 3$ replicates is plotted in solid lines. Controls in gray (naive cells in light gray, cells exiting pluripotency in dark gray) and Taxol-treated cells in green (naive cells in light green, exiting cells in dark green).

(B) Quantification of P-Aurora B intensity in naive ESCs treated with DMSO or 0.5 μ M Taxol and exiting ESCs treated with DMSO or 0.5 μ M Taxol. Mean \pm SD. $N = 3$ replicates.

(C) Immunofluorescence showing the number of bridges in naive or 48 h exiting ESCs treated with DMSO or 0.5 μ M Taxol. Bridges: pink asterisks. Scale bars: 10 μ m.

(D) Quantification of the number of bridges per cell in naive ESCs treated with DMSO or 0.5 μ M Taxol or 48 h exiting ESCs treated with DMSO or 0.5 μ M Taxol. Mean \pm SD. $N = 3$ replicates.

(E) Immunofluorescence showing the number of bridges in naive ESCs treated with DMSO or various concentrations of nocodazole. Bridges: pink asterisks. Scale bars: 10 μ m.

(F) Quantification of the number of bridges per cell in naive ESCs treated with DMSO or various concentrations of nocodazole. Mean \pm SD. $N = 3$ replicates.

(G) Graph showing the duration of abscission in naive ESCs in several conditions: untreated and treated with 2 μ M ZM447439 (similar to Figure 1H), expressing StableMARK (from Figure 3F), and expressing StableMARK and treated with 2 μ M ZM447439 (from Figure 4F). Mean \pm SD.

(Figures 7A and 7B), which mirrored the stability of microtubules (Figures 3C–3J). Live cell imaging confirmed that MCAK was recruited to the middle of the bridge shortly after bridge formation, then transiently disappeared from the arms and remained as a faint signal at the midbody (Figure S6A; Video 8). As a side note, in fixed cells, the presence of MCAK at the midbody cannot be detected (Figure 7A), probably due to a lack of penetration of the antibody in the so-called dark zone. Shortly before abscission, MCAK was seen more broadly across the bridge again (Figure S6A; Video 9). Importantly, when Aurora B activity was inhibited 2 h after bridge formation, the lowest point of MCAK recruitment (Figure 7B), MCAK recruitment on the bridge increased (Figures S6B and S6C). Consistently, when microtubules were stabilized using Taxol, MCAK recruitment dropped (Figures 7C and 7D). Late bridges showed clear spatial separation between MCAK and acetylated tubulin, with one arm en-

riched in acetylated tubulin and the other enriched in MCAK in 29.7% naive ESCs and 32.3% exit ESCs (Figures 7E and 7F). Finally, to demonstrate that MCAK recruitment is sufficient to accelerate abscission, we treated naive ESCs with the MCAK activator UMK57.⁵² Cells treated with UMK57 showed accelerated abscission (Figure 7G). Altogether, these data show that the stabilization of microtubules leads to low MCAK recruitment at the bridge and slow abscission.

DISCUSSION

In this paper, we investigated the molecular mechanisms for the regulation of abscission dynamics in a physiological developmental context. Our data show that apart from having a vital role in stalling abscission upon chromosome segregation errors,^{24,38,41,43,53–57} Aurora B kinase also regulates the dynamics of abscission during exit from naive pluripotency. This is consistent with Aurora B activity maintaining cytoplasmic bridges in the

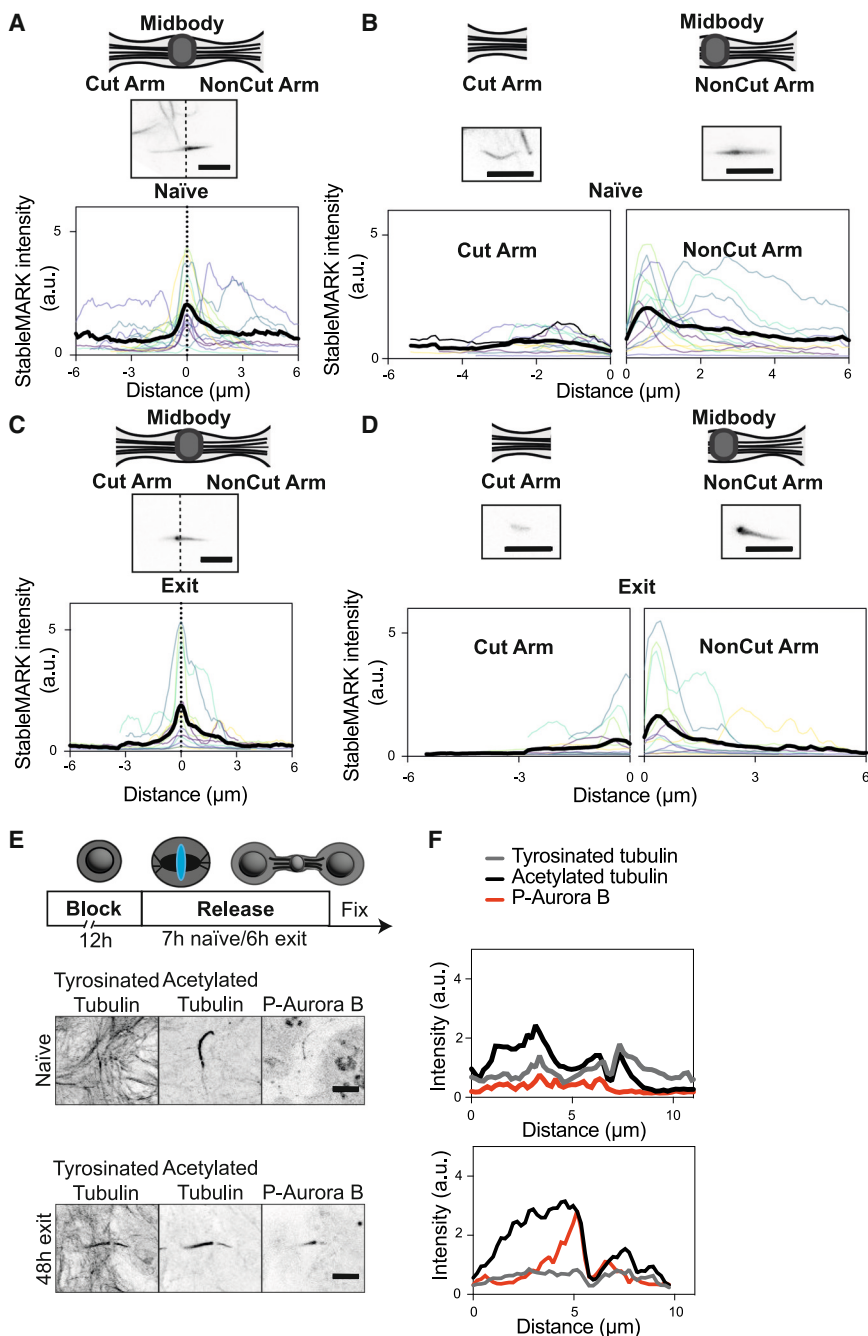


Figure 6. Bridges break at location of low microtubule stability

(A) Top: a cytoplasmic bridge with the midbody in the center and the cut arm and non-cut arm before abscission. Bottom: graph showing the intensity of StableMARK along the two arms of bridges of naïve ESCs before abscission (cut arm on the left, non-cut arm on the right). Insets show examples. Scale bars: 5 μm . N = 3 replicates.

(B) Top: a cytoplasmic bridge with the midbody in the center and the cut arm and non-cut arm after abscission. Bottom: graph showing the intensity of StableMARK along the two arms of bridges of naïve ESCs after abscission (cut arm on the left, non-cut arm on the right). Insets show examples. Scale bars: 5 μm . N = 3 replicates.

(C) Top: a cytoplasmic bridge with the midbody in the center and the cut arm and non-cut arm before abscission. Bottom: graph showing the intensity of StableMARK along the two arms of bridges of 48 h exiting ESCs before abscission (cut arm on the left, non-cut arm on the right). Insets show examples. Scale bars: 5 μm . N = 3 replicates.

(D) Top: a cytoplasmic bridge with the midbody in the center and the cut arm and non-cut arm after abscission. Bottom: graph showing the intensity of StableMARK along the two arms of bridges of 48 h exiting ESCs after abscission (cut arm on the left, non-cut arm on the right). Insets show examples. Scale bars: 5 μm . N = 3 replicates.

(E) Top: schematic of the experimental setup. Immunofluorescence showing the localization of tyrosinated tubulin, acetylated tubulin, and P-Aurora B in naïve and 48 h exiting ESCs 7 h after release (naïve) or 6 h after release (exit). Scale bars: 5 μm .

(F) Line plot showing the intensity of tyrosinated tubulin, acetylated tubulin, and P-Aurora B in the two examples from (E). Representative example from N = 3 replicates.

early mouse embryo⁴⁰ or in human cells, even in the absence of mitotic defects.⁴³ Using precise temporal dissection of bridge maturation with fixed and live cell imaging, we showed that Aurora B amount and activity decrease as the bridge matures and are higher in naïve cells compared to exit cells and that inhibiting Aurora B activity drastically accelerates abscission (Figure 1).

What could explain the increased Aurora B activity at the bridge in naïve cells? Our data suggest a dual model, whereby naïve cells have higher amounts of Aurora B at the bridge and increased

activity of Aurora B. At anaphase, Aurora B is transported from the kinetochore along the microtubules⁵⁸ by the motor KIF20A.⁵⁹ Our data suggest increased transport or stability of Aurora B on the cytoplasmic bridge in naïve cells. Several hypotheses could explain this result. First, there is a global decrease in the expression levels of KIF20A during exit from naïve pluripotency,^{60,61} which could explain the enhanced transport of Aurora B to the bridge in naïve cells. Second, the amount of microtubules present in the bridge can directly impact the abundance and activity of Aurora B⁶²; the increased stability of microtubules in naïve cells could promote the continuous recruitment and activation of Aurora B. Third, in cancer cells, it has been proposed that Aurora B is degraded at the bridge to promote abscission,⁹ which could also be at play here.

We demonstrate that Aurora B plays a role in maintaining pluripotency (Figure 2). Indeed, a short inhibition of Aurora B accelerates the exit from naïve pluripotency. We previously showed

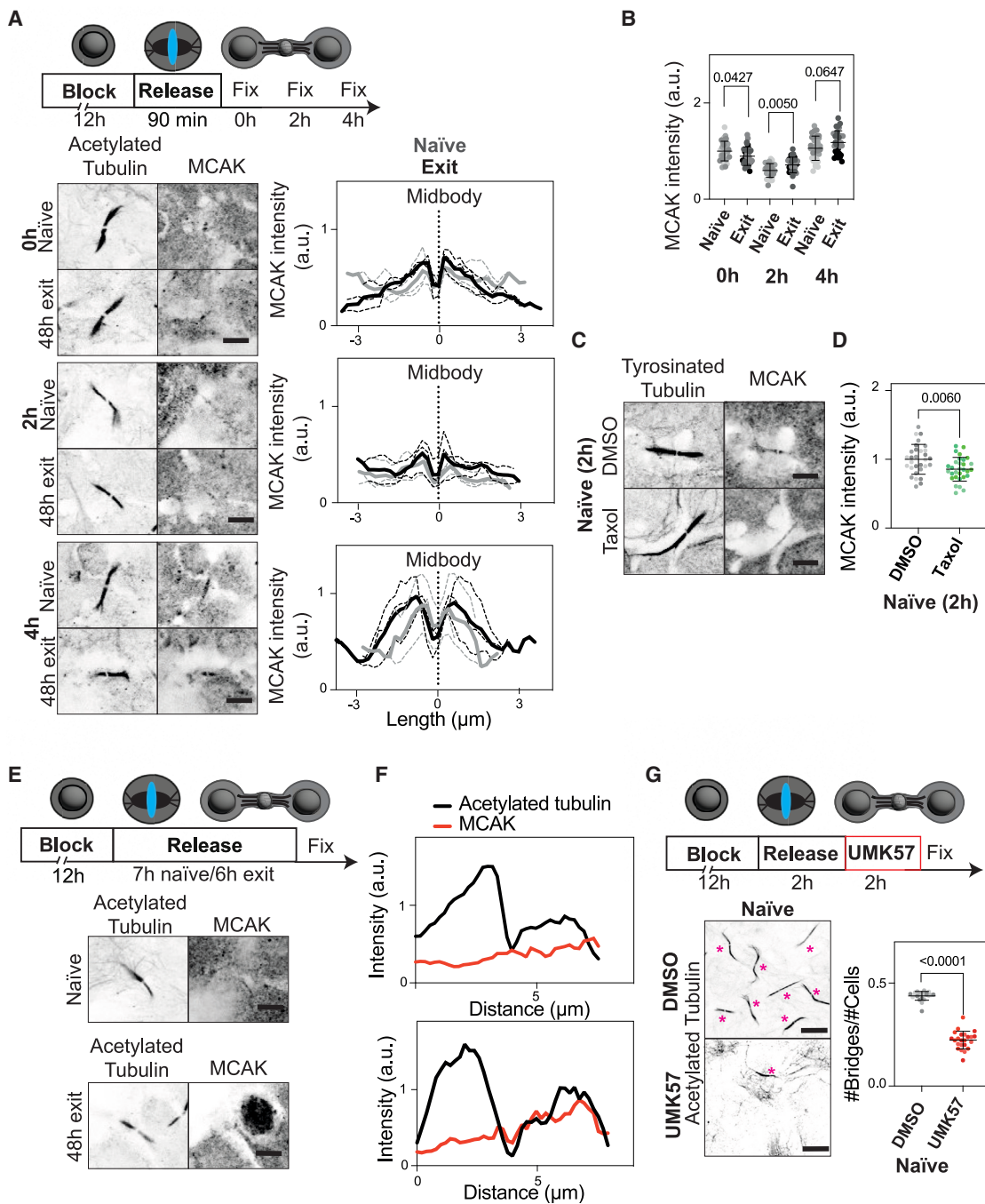


Figure 7. MCAK is excluded from stable microtubules

(A) Top: schematic of the experimental setup. Bottom left: immunofluorescence showing the localization of MCAK in naïve and 48 h exiting ESCs during bridge maturation at bridge formation (0h), 2 h after bridge formation (2h), and 4 h after bridge formation (4h). Scale bars: 5 μm . Bottom right: line scans showing the intensity of MCAK along the length of bridges. The mean of $n = 10$ cells per replicate is plotted in dotted lines, and the mean of $N = 3$ replicates is plotted in solid lines. Naïve cells are shown in gray, cells exiting pluripotency are shown in black.

(B) Quantification of MCAK intensity in naïve and exiting ESCs. Mean \pm SD. $N = 3$ replicates.

(C) Immunofluorescence showing the localization of MCAK in naïve ESCs treated with DMSO or 0.5 μM Taxol 2 h after bridge formation. Scale bars: 5 μm .

(D) Quantification of MCAK intensity in naïve ESCs treated with DMSO or 0.5 μM Taxol 2 h after bridge formation. Mean \pm SD. $N = 3$ replicates.

(E) Top: schematic of the experimental setup. Immunofluorescence showing the localization of acetylated tubulin and MCAK in naïve and 48 h exiting ESCs 7 h after release (naïve) or 6 h after release (exit). Scale bars: 5 μm .

(legend continued on next page)

that abscission speed is tightly coupled to cell fate.¹ Thus, Aurora B could have an indirect effect on cell fate by regulating abscission; however, our data do not exclude a model in which Aurora B also directly controls cell fate, and further studies will be necessary to untangle these two possibilities.

We show that Aurora B regulates the duration of abscission by maintaining microtubule stability (Figures 3 and 4). We do not know how Aurora B activity controls microtubule dynamics or stability, but several hypotheses can be proposed. First, Aurora B could regulate enzymes that modify tubulin post-translationally such as α TAT1^{63,64} (the acetyltransferase responsible for tubulin acetylation at Lysine 40) or microtubule deacetylases HDAC-6⁶⁵ or SIRT2.⁶⁶ Tubulin acetylation has in turn been shown to protect microtubules against mechanical injuries, perhaps leading to increased stability.⁶⁷ Second, Aurora B inactivates MCAK by phosphorylation.^{48,68} Thus, Aurora B could promote microtubule stability by inhibiting MCAK-dependent microtubule depolymerization. Third, it is likely that Aurora B has targets other than microtubules, as it controls abscission through the regulation of ESCRT in other model systems.²⁴

We demonstrate that stable microtubules inhibit abscission (Figures 5 and 6). How could stable microtubules specifically delay abscission? We show that Aurora B activity and microtubule stabilization lead to a decrease in MCAK recruitment to the bridge (Figure 7). Crucially, we see a spatial separation of the different players, with P-Aurora B and acetylated microtubules on one arm and MCAK on the other (Figures 6 and 7), suggesting that MCAK actively depolymerizes non-acetylated microtubules when Aurora B activity is low. This also suggests that Aurora B could control abscission dynamics by influencing both MCAK activity^{48,68} and its recruitment. Finally, we show that hyper-activating MCAK is sufficient to drive faster abscission. Thus, we propose that the stabilization of microtubules prevents the primary constriction of the bridge by rendering them insensitive to MCAK-driven microtubule depolymerization. To our knowledge, this is the first report of MCAK involvement in abscission. Our model is also compatible with the idea that stable microtubules are less sensitive to mechanical stress⁶⁹; thus, stable microtubules could also promote the structural integrity of the bridge.

Overall, our results demonstrate that the activity of Aurora B kinase can regulate abscission dynamics through the regulation of microtubule stability, which hinders MCAK recruitment and microtubule depolymerization. In contrast to traditional models wherein microtubules are passive remnants of the mitotic spindle, our study identifies microtubules themselves as a main driver in abscission dynamics.

Limitations of the study

Our results demonstrate that in mouse ESCs, Aurora B controls microtubule stability. We did not explore the link between Aurora B and microtubule stability. Furthermore, here, we explore only how Aurora B controls abscission through microtubule stability;

however, in other cell types, Aurora B controls abscission through direct or indirect modulation of ESCRT-III localization,^{24,37,70} and it is likely that these mechanisms are also at play in ESCs, in parallel with the modulation of microtubule stability.

RESOURCE AVAILABILITY

Lead contact

Further information and requests for resources and reagents should be directed to and will be fulfilled by the lead contact, Agathe Chaigne (a.e.d.chaigne@uu.nl).

Material availability

No new materials were generated in this study.

Data and code availability

- Data

The data generated for this study will be available on the data management platform Yoda of Utrecht University according to FAIR guidelines upon publication.

- Code

The code is described in the [STAR Methods](#) and is openly available on GitHub.

- Other items

Any additional information required to reanalyze the data reported in this paper is available from the [lead contact](#) upon request.

ACKNOWLEDGMENTS

We would like to thank all the members of the Chaigne lab and the whole department of Cell Biology, Neurobiology and Biophysics at Utrecht University, in particular Anna Akhmanova for helpful discussions. We thank Benjamin P. Bouchet (Akhmanova lab, Utrecht University) for his advice on UMK57. We thank Joyce Meiring (Akhmanova lab, Utrecht University) for sharing pTT5 SII-GFP-MCAK. We also would like to thank Gautam Dey (European Molecular Biology Laboratory), Susanne Lens (University Medical Center Utrecht), Marie-Emilie Terret (Collège de France), and Ruby Peters (Cambridge University) for feedback on the manuscript.

This work was supported by Utrecht University and NWO (NWO-Vidi to A.C.), the European Research Council (ERC Consolidator Grant 819219 to L.C.K.), and the Centre for Living Technologies, a part of the Alliance TU/e, WUR, UU, and UMC Utrecht (Eindhoven University of Technology, Wageningen University & Research, Utrecht University, and University Medical Center Utrecht; www.ewuu.nl).

AUTHOR CONTRIBUTIONS

S.K. performed most of the experiments and analysis. A.O. performed some of the StableMARK experiments and analysis. E.v.B. was involved in the experiments and analysis of the characterization of the different populations of microtubules in fixed samples. M.K.I. was involved in the imaging and analysis of fixed and live microtubules. W.N. was involved in the imaging and analysis of Aurora B and P-Aurora B. L.C.K. was involved in the conceptualization. E.A.K. developed the pipeline for the kymographs. A.C. performed some of the qPCRs and clonogenicity assays and the conceptualization, supervision, and funding acquisition. All authors discussed the data and the manuscript.

DECLARATION OF INTERESTS

The authors declare no competing interests.

(F) Line plot showing the intensity of acetylated tubulin and MCAK in the two examples from (G). Representative example from $N = 3$ replicates.

(G) Top: schematic of the experimental setup. Left: immunofluorescence showing the number of bridges in naive ESCs treated with DMSO or 2 μ M UMK57. Bridges: pink asterisks. Scale bars: 10 μ m. Right: quantification of the number of bridges per cell in naive ESCs treated with DMSO or UMK57. Mean \pm SD. $N = 3$ replicates.

STAR★METHODS

Detailed methods are provided in the online version of this paper and include the following:

- **KEY RESOURCES TABLE**
- **EXPERIMENTAL MODEL AND STUDY PARTICIPANT DETAILS**
- **METHOD DETAILS**
 - Cell culture and transfection
 - Drug treatment
 - Immunofluorescence
 - Live imaging
 - Colony-forming assay
- **QUANTIFICATION AND STATISTICAL ANALYSIS**
 - Image analysis
 - Statistical analysis and data display

SUPPLEMENTAL INFORMATION

Supplemental information can be found online at <https://doi.org/10.1016/j.celrep.2025.115238>.

Received: March 11, 2024

Revised: October 11, 2024

Accepted: January 6, 2025

Published: January 23, 2025

REFERENCES

1. Chaigne, A., Labouesse, C., White, I.J., Agnew, M., Hannezo, E., Chalut, K.J., and Paluch, E.K. (2020). Abscission Couples Cell Division to Embryonic Stem Cell Fate. *Dev. Cell* 55, 195–208.e5. <https://doi.org/10.1016/j.devcel.2020.09.001>.
2. Zhu, C., and Jiang, W. (2005). Cell cycle-dependent translocation of PRC1 on the spindle by Kif4 is essential for midzone formation and cytokinesis. *Proc. Natl. Acad. Sci. USA* 102, 343–348. <https://doi.org/10.1073/pnas.0408438102>.
3. Jiang, W., Jimenez, G., Wells, N.J., Hope, T.J., Wahl, G.M., Hunter, T., and Fukunaga, R. (1998). PRC1: A Human Mitotic Spindle–Associated CDK Substrate Protein Required for Cytokinesis. *Mol. Cell* 2, 877–885. [https://doi.org/10.1016/S1097-2765\(00\)80302-0](https://doi.org/10.1016/S1097-2765(00)80302-0).
4. Kurasawa, Y., Earnshaw, W.C., Mochizuki, Y., Dohmae, N., and Todokoro, K. (2004). Essential roles of KIF4 and its binding partner PRC1 in organized central spindle midzone formation. *EMBO J.* 23, 3237–3248. <https://doi.org/10.1038/sj.emboj.7600347>.
5. White, E.A., and Glotzer, M. (2012). Centralspindlin: At the heart of cytokinesis. *Cytoskeleton* 69, 882–892. <https://doi.org/10.1002/cm.21065>.
6. Kaitna, S., Mendoza, M., Jantsch-Plunger, V., and Glotzer, M. (2000). Incep and an Aurora-like kinase form a complex essential for chromosome segregation and efficient completion of cytokinesis. *Curr. Biol.* 10, 1172–1181. [https://doi.org/10.1016/S0960-9822\(00\)00721-1](https://doi.org/10.1016/S0960-9822(00)00721-1).
7. Peterman, E., and Prekeris, R. (2019). The postmitotic midbody: Regulating polarity, stemness, and proliferation. *J. Cell Biol.* 218, 3903–3911. <https://doi.org/10.1083/jcb.201906148>.
8. Hu, C.-K., Coughlin, M., and Mitchison, T.J. (2012). Midbody assembly and its regulation during cytokinesis. *Mol. Biol. Cell* 23, 1024–1034. <https://doi.org/10.1091/mbc.e11-08-0721>.
9. Halcrow, E.F.J., Mazza, R., Diversi, A., Enright, A., and D'Avino, P.P. (2022). Midbody Proteins Display Distinct Dynamics during Cytokinesis. *Cells* 11, 3337. <https://doi.org/10.3390/cells11213337>.
10. Mierwza, B., and Gerlich, D.W. (2014). Cytokinetic abscission: molecular mechanisms and temporal control. *Dev. Cell* 31, 525–538. <https://doi.org/10.1016/j.devcel.2014.11.006>.
11. Bastos, R.N., and Barr, F.A. (2010). Plk1 negatively regulates Cep55 recruitment to the midbody to ensure orderly abscission. *J. Cell Biol.* 191, 751–760. <https://doi.org/10.1083/jcb.201008108>.
12. Carlton, J.G., Agromayor, M., and Martin-Serrano, J. (2008). Differential requirements for Alix and ESCRT-III in cytokinesis and HIV-1 release. *Proc. Natl. Acad. Sci. USA* 105, 10541–10546. <https://doi.org/10.1073/pnas.0802008105>.
13. Lee, H.H., Elia, N., Ghirlando, R., Lippincott-Schwartz, J., and Hurley, J.H. (2008). Midbody Targeting of the ESCRT Machinery by a Noncanonical Coiled Coil in CEP55. *Science* 322, 576–580. <https://doi.org/10.1126/science.1162042>.
14. Christ, L., Wenzel, E.M., Liestøl, K., Raiborg, C., Campsteijn, C., and Stenmark, H. (2016). ALIX and ESCRT-I/II function as parallel ESCRT-III recruiters in cytokinetic abscission. *JCB (J. Cell Biol.)* 212, 499–513. <https://doi.org/10.1083/jcb.201507009>.
15. Goliand, I., Nachmias, D., Gershony, O., and Elia, N. (2014). Inhibition of ESCRT-II–CHMP6 interactions impedes cytokinetic abscission and leads to cell death. *MBoC* 25, 3740–3748. <https://doi.org/10.1091/mbo.e14-08-1317>.
16. Morita, E., Sandrin, V., Chung, H.-Y., Morham, S.G., Gygi, S.P., Rodesch, C.K., and Sundquist, W.I. (2007). Human ESCRT and ALIX proteins interact with proteins of the midbody and function in cytokinesis. *EMBO J.* 26, 4215–4227. <https://doi.org/10.1038/sj.emboj.7601850>.
17. Katoh, K., Shibata, H., Suzuki, H., Nara, A., Ishidoh, K., Kominami, E., Yoshimori, T., and Maki, M. (2003). The ALG-2-interacting Protein Alix Associates with CHMP4b, a Human Homologue of Yeast Snf7 That Is Involved in Multivesicular Body Sorting. *J. Biol. Chem.* 278, 39104–39113. <https://doi.org/10.1074/jbc.M301604200>.
18. Katoh, K., Shibata, H., Hatta, K., and Maki, M. (2004). CHMP4b is a major binding partner of the ALG-2-interacting protein Alix among the three CHMP4 isoforms. *Arch. Biochem. Biophys.* 421, 159–165. <https://doi.org/10.1016/j.abb.2003.09.038>.
19. Karasmanis, E.P., Hwang, D., Nakos, K., Bowen, J.R., Angelis, D., and Spiliotis, E.T. (2019). A Septin Double Ring Controls the Spatiotemporal Organization of the ESCRT Machinery in Cytokinetic Abscission. *Curr. Biol.* 29, 2174–2182.e7. <https://doi.org/10.1016/j.cub.2019.05.050>.
20. Merigliano, C., Burla, R., La Torre, M., Del Giudice, S., Teo, H., Liew, C.W., Chojnowski, A., Goh, W.I., Olmos, Y., Maccaroni, K., et al. (2021). AKTIP interacts with ESCRT I and is needed for the recruitment of ESCRT III subunits to the midbody. *PLoS Genet.* 17, e1009757. <https://doi.org/10.1371/journal.pgen.1009757>.
21. Addi, C., Presle, A., Frémont, S., Cuvelier, F., Rocancourt, M., Milin, F., Schmutz, S., Chamot-Rooke, J., Douché, T., Duchateau, M., et al. (2020). The Flemmingsome reveals an ESCRT-to-membrane coupling via ALIX/syntenin/syndecan-4 required for completion of cytokinesis. *Nat. Commun.* 11, 1941. <https://doi.org/10.1038/s41467-020-15205-z>.
22. Mierwza, B.E., Chiartini, N., Redondo-Morata, L., von Filseck, J.M., König, J., Larios, J., Poser, I., Müller-Reichert, T., Scheuring, S., Roux, A., and Gerlich, D.W. (2017). Dynamic subunit turnover in ESCRT-III assemblies is regulated by Vps4 to mediate membrane remodelling during cytokinesis. *Nat. Cell Biol.* 19, 787–798.
23. Guizetti, J., Schermelleh, L., Mäntler, J., Maar, S., Poser, I., Leonhardt, H., Müller-Reichert, T., and Gerlich, D.W. (2011). Cortical Constriction During Abscission Involves Helices of ESCRT-III-Dependent Filaments. *Science* 331, 1616–1620. <https://doi.org/10.1126/science.1201847>.
24. Carlton, J.G., Caballe, A., Agromayor, M., Kloc, M., and Martin-Serrano, J. (2012). ESCRT-III Governs the Aurora B-Mediated Abscission Checkpoint Through CHMP4C. *Science* 336, 220–225. <https://doi.org/10.1126/science.1220007>.
25. Addi, C., Bai, J., and Echard, A. (2018). Actin, microtubule, septin and ESCRT filament remodeling during late steps of cytokinesis. *Curr. Opin. Cell Biol.* 50, 27–34. <https://doi.org/10.1016/j.ceb.2018.01.007>.
26. Frémont, S., Hammich, H., Bai, J., Wioland, H., Klinkert, K., Rocancourt, M., Kikuti, C., Stroebel, D., Romet-Lemonne, G., Pylypenko, O., et al.

- (2017). Oxidation of F-actin controls the terminal steps of cytokinesis. *Nat. Commun.* 8, 14528. <https://doi.org/10.1038/ncomms14528>.
27. Dambourret, D., Machicoane, M., Chesneau, L., Sachse, M., Rocancourt, M., El Marjou, A., Formstecher, E., Salomon, R., Goud, B., and Echard, A. (2011). Rab35 GTPase and OCRL phosphatase remodel lipids and F-actin for successful cytokinesis. *Nat. Cell Biol.* 13, 981–988. <https://doi.org/10.1038/hcb2279>.
 28. Kouranti, I., Sachse, M., Arouche, N., Goud, B., and Echard, A. (2006). Rab35 Regulates an Endocytic Recycling Pathway Essential for the Terminal Steps of Cytokinesis. *Curr. Biol.* 16, 1719–1725. <https://doi.org/10.1016/j.cub.2006.07.020>.
 29. Advedessian, T., Frémont, S., and Echard, A. (2024). Cytokinetic abscission requires actin-dependent microtubule severing. *Nat. Commun.* 15, 1949. <https://doi.org/10.1038/s41467-024-46062-9>.
 30. Yang, D., Rismanchi, N., Renvoisé, B., Lippincott-Schwartz, J., Blackstone, C., and Hurley, J.H. (2008). Structural basis for midbody targeting of spastin by the ESCRT-III protein CHMP1B. *Nat. Struct. Mol. Biol.* 15, 1278–1286. <https://doi.org/10.1038/nsmb.1512>.
 31. Reid, E., Connell, J., Edwards, T.L., Duley, S., Brown, S.E., and Sanderson, C.M. (2005). The hereditary spastic paraparesis protein spastin interacts with the ESCRT-III complex-associated endosomal protein CHMP1B. *Hum. Mol. Genet.* 14, 19–38. <https://doi.org/10.1093/hmg/ddi003>.
 32. Connell, J.W., Lindon, C., Luzio, J.P., and Reid, E. (2009). Spastin Couples Microtubule Severing to Membrane Traffic in Completion of Cytokinesis and Secretion. *Traffic* 10, 42–56. <https://doi.org/10.1111/j.1600-0854.2008.00847.x>.
 33. Vietri, M., Schink, K.O., Campsteijn, C., Wegner, C.S., Schultz, S.W., Christ, L., Thoresen, S.B., Brech, A., Raiborg, C., and Stenmark, H. (2015). Spastin and ESCRT-III coordinate mitotic spindle disassembly and nuclear envelope sealing. *Nature* 522, 231–235. <https://doi.org/10.1038/nature14408>.
 34. Wenzel, D.M., Mackay, D.R., Skalicky, J.J., Paine, E.L., Miller, M.S., Ullman, K.S., and Sundquist, W.I. (2022). Comprehensive analysis of the human ESCRT-III-MIT domain interactome reveals new cofactors for cytokinetic abscission. *Elife* 11, e77779. <https://doi.org/10.7554/elife.77779>.
 35. Matsuo, M., Shimodaira, T., Kasama, T., Hata, Y., Echigo, A., Okabe, M., Arai, K., Makino, Y., Niwa, S.-I., Saya, H., and Kishimoto, T. (2013). Katanin p60 Contributes to Microtubule Instability around the Midbody and Facilitates Cytokinesis in Rat Cells. *PLoS One* 8, e80392. <https://doi.org/10.1371/journal.pone.0080392>.
 36. Capalbo, L., Montembault, E., Takeda, T., Bassi, Z.I., Glover, D.M., and D'Avino, P.P. (2012). The chromosomal passenger complex controls the function of endosomal sorting complex required for transport-III Snf7 proteins during cytokinesis. *Open Biol.* 2, 120070. <https://doi.org/10.1098/rsob.120070>.
 37. Strohacker, L.K., Mackay, D.R., Whitney, M.A., Couldwell, G.C., Sundquist, W.I., and Ullman, K.S. (2021). Identification of abscission checkpoint bodies as structures that regulate ESCRT factors to control abscission timing. *Elife* 10, e63743. <https://doi.org/10.7554/elife.63743>.
 38. Thoresen, S.B., Campsteijn, C., Vietri, M., Schink, K.O., Liestøl, K., Andersen, J.S., Raiborg, C., and Stenmark, H. (2014). ANCHR mediates Aurora-B-dependent abscission checkpoint control through retention of VPS4. *Nat. Cell Biol.* 16, 550–560. <https://doi.org/10.1038/ncb2959>.
 39. Mathieu, J., Cauvin, C., Moch, C., Radford, S.J., Sampaio, P., Perdigoto, C.N., Schweigert, F., Bardin, A.J., Sunkel, C.E., McKim, K., et al. (2013). Aurora B and Cyclin B Have Opposite Effects on the Timing of Cytokinesis Abscission in Drosophila Germ Cells and in Vertebrate Somatic Cells. *Dev. Cell* 26, 250–265. <https://doi.org/10.1016/j.devcel.2013.07.005>.
 40. Zenker, J., White, M.D., Templin, R.M., Parton, R.G., Thorn-Seshold, O., Bissiere, S., and Plachta, N. (2017). A microtubule-organizing center directing intracellular transport in the early mouse embryo. *Science* 357, 925–928. <https://doi.org/10.1126/science.aam9335>.
 41. Fung, S.Y.S., Kitagawa, M., Liao, P.-J., Wong, J., and Lee, S.H. (2017). Opposing Activities of Aurora B Kinase and B56-PP2A Phosphatase on MKlp2 Determine Abscission Timing. *Curr. Biol.* 27, 78–86. <https://doi.org/10.1016/j.cub.2016.10.042>.
 42. Yasui, Y., Urano, T., Kawajiri, A., Nagata, K.i., Tatsuka, M., Saya, H., Furukawa, K., Takahashi, T., Izawa, I., and Inagaki, M. (2004). Autophosphorylation of a Newly Identified Site of Aurora-B Is Indispensable for Cytokinesis. *J. Biol. Chem.* 279, 12997–13003. <https://doi.org/10.1074/jbc.M311128200>.
 43. Steigemann, P., Wurzenberger, C., Schmitz, M.H.A., Held, M., Guizetti, J., Maar, S., and Gerlich, D.W. (2009). Aurora B-Mediated Abscission Checkpoint Protects against Tetraploidization. *Cell* 136, 473–484. <https://doi.org/10.1016/j.cell.2008.12.020>.
 44. Cohen, P., Holmes, C.F., and Tsukitani, Y. (1990). Okadaic acid: a new probe for the study of cellular regulation. *Trends Biochem. Sci.* 15, 98–102. [https://doi.org/10.1016/0968-0004\(90\)90192-E](https://doi.org/10.1016/0968-0004(90)90192-E).
 45. Mulas, C., Kalkan, T., and Smith, A. (2017). NODAL Secures Pluripotency upon Embryonic Stem Cell Progression from the Ground State. *Stem Cell Rep.* 9, 77–91. <https://doi.org/10.1016/j.stemcr.2017.05.033>.
 46. Strawbridge, S.E., Blanchard, G.B., Smith, A., Kugler, H., and Martello, G. (2020). Embryonic stem cells commit to differentiation by symmetric divisions following a variable lag period (Developmental Biology) <https://doi.org/10.1101/2020.06.17.157578>.
 47. Nunes Bastos, R., Gandhi, S.R., Baron, R.D., Gruneberg, U., Nigg, E.A., and Barr, F.A. (2013). Aurora B suppresses microtubule dynamics and limits central spindle size by locally activating KIF4A. *J. Cell Biol.* 202, 605–621. <https://doi.org/10.1083/jcb.201301094>.
 48. Lan, W., Zhang, X., Kline-Smith, S.L., Rosasco, S.E., Barrett-Wilt, G.A., Shabanowitz, J., Hunt, D.F., Walczak, C.E., and Stukenberg, P.T. (2004). Aurora B Phosphorylates Centromeric MCAK and Regulates Its Localization and Microtubule Depolymerization Activity. *Curr. Biol.* 14, 273–286. <https://doi.org/10.1016/j.cub.2004.01.055>.
 49. Akhmanova, A., and Kapitein, L.C. (2022). Mechanisms of microtubule organization in differentiated animal cells. *Nat. Rev. Mol. Cell Biol.* 23, 541–558. <https://doi.org/10.1038/s41580-022-00473-y>.
 50. Jansen, K.I., Iwanski, M.K., Burute, M., and Kapitein, L.C. (2023). A live-cell marker to visualize the dynamics of stable microtubules throughout the cell cycle. *J. Cell Biol.* 222, e202106105. <https://doi.org/10.1083/jcb.202106105>.
 51. Ettinger, A.W., Wilsch-Bräuninger, M., Marzesco, A.-M., Bickle, M., Lohmann, A., Maliga, Z., Karbanová, J., Corbeil, D., Hyman, A.A., and Hüttnér, W.B. (2011). Proliferating versus differentiating stem and cancer cells exhibit distinct midbody-release behaviour. *Nat. Commun.* 2, 503. <https://doi.org/10.1038/ncomms1511>.
 52. Orr, B., Talje, L., Liu, Z., Kwok, B.H., and Compton, D.A. (2016). Adaptive Resistance to an Inhibitor of Chromosomal Instability in Human Cancer Cells. *Cell Rep.* 17, 1755–1763. <https://doi.org/10.1016/j.celrep.2016.10.030>.
 53. Pike, T., Brownlow, N., Kjaer, S., Carlton, J., and Parker, P.J. (2016). PKC ϵ switches Aurora B specificity to exit the abscission checkpoint. *Nat. Commun.* 7, 13853. <https://doi.org/10.1038/ncomms13853>.
 54. Amaral, N., Vendrell, A., Funaya, C., Idrissi, F.-Z., Maier, M., Kumar, A., Neurohr, G., Colomina, N., Torres-Rosell, J., Geli, M.-I., and Mendoza, M. (2016). The Aurora-B-dependent NoCut checkpoint prevents damage of anaphase bridges after DNA replication stress. *Nat. Cell Biol.* 18, 516–526. <https://doi.org/10.1038/ncb3343>.
 55. Mackay, D.R., Makise, M., and Ullman, K.S. (2010). Defects in nuclear pore assembly lead to activation of an Aurora B-mediated abscission checkpoint. *J. Cell Biol.* 191, 923–931. <https://doi.org/10.1083/jcb.201007124>.
 56. Mackay, D.R., and Ullman, K.S. (2015). ATR and a Chk1-Aurora B pathway coordinate postmitotic genome surveillance with cytokinetic abscission. *MBoC* 26, 2217–2226. <https://doi.org/10.1091/mbo.E14-11-1563>.

57. Watson, L., Soliman, T.N., Davis, K., Kelly, J., Lockwood, N., Yang, X., Lynham, S., Scott, J.D., Crossland, V., McDonald, N.Q., et al. (2021). Co-ordinated control of the Aurora B abscission checkpoint by PKC ϵ complex assembly, midbody recruitment and retention. *Biochem. J.* 478, 2247–2263. <https://doi.org/10.1042/BCJ20210283>.
58. Hadders, M.A., and Lens, S.M.A. (2022). Changing places: Chromosomal Passenger Complex relocation in early anaphase. *Trends Cell Biol.* 32, 165–176. <https://doi.org/10.1016/j.tcb.2021.09.008>.
59. Adriaans, I.E., Hooikaas, P.J., Aher, A., Vromans, M.J.M., van Es, R.M., Grigoriev, I., Akhmanova, A., and Lens, S.M.A. (2020). MKLP2 Is a Motile Kinesin that Transports the Chromosomal Passenger Complex during Anaphase. *Curr. Biol.* 30, 2628–2637.e9. <https://doi.org/10.1016/j.cub.2020.04.081>.
60. Kalkan, T., Olova, N., Roode, M., Mulas, C., Lee, H.J., Nett, I., Marks, H., Walker, R., Stunnenberg, H.G., Lilley, K.S., et al. (2017). Tracking the embryonic stem cell transition from ground state pluripotency. *Development* 144, 1221–1234. <https://doi.org/10.1242/dev.142711>.
61. Yang, P., Humphrey, S.J., Cinghu, S., Pathania, R., Oldfield, A.J., Kumar, D., Perera, D., Yang, J.Y.H., James, D.E., Mann, M., and Jothi, R. (2019). Multi-omic Profiling Reveals Dynamics of the Phased Progression of Pluripotency. *Cell Syst.* 8, 427–445.e10. <https://doi.org/10.1016/j.cels.2019.03.012>.
62. Noujaim, M., Bechstedt, S., Wieczorek, M., and Brouhard, G.J. (2014). Microtubules Accelerate the Kinase Activity of Aurora-B by a Reduction in Dimensionality. *PLoS One* 9, e86786. <https://doi.org/10.1371/journal.pone.0086786>.
63. Akella, J.S., Wloga, D., Kim, J., Starostina, N.G., Lyons-Abbott, S., Morrisette, N.S., Dougan, S.T., Kipreos, E.T., and Gaertig, J. (2010). MEC-17 is an α -tubulin acetyltransferase. *Nature* 467, 218–222. <https://doi.org/10.1038/nature09324>.
64. Kalebic, N., Sorrentino, S., Perlas, E., Bolasco, G., Martinez, C., and Heppenstall, P.A. (2013). α TAT1 is the major α -tubulin acetyltransferase in mice. *Nat. Commun.* 4, 1962. <https://doi.org/10.1038/ncomms2962>.
65. Hubbert, C., Guardiola, A., Shao, R., Kawaguchi, Y., Ito, A., Nixon, A., Yoshida, M., Wang, X.-F., and Yao, T.-P. (2002). HDAC6 is a microtubule-associated deacetylase. *Nature* 417, 455–458. <https://doi.org/10.1038/417455a>.
66. North, B.J., Marshall, B.L., Borra, M.T., Denu, J.M., and Verdin, E. (2003). The Human Sir2 Ortholog, SIRT2, Is an NAD+-Dependent Tubulin Deace-
- tylase. *Mol. Cell* 11, 437–444. [https://doi.org/10.1016/S1097-2765\(03\)00038-8](https://doi.org/10.1016/S1097-2765(03)00038-8).
67. Portran, D., Schaedel, L., Xu, Z., Théry, M., and Nachury, M.V. (2017). Tubulin acetylation protects long-lived microtubules against mechanical ageing. *Nat. Cell Biol.* 19, 391–398. <https://doi.org/10.1038/ncb3481>.
68. Andrews, P.D., Ovechkina, Y., Morrice, N., Wagenbach, M., Duncan, K., Wordeman, L., and Swedlow, J.R. (2004). Aurora B Regulates MCAK at the Mitotic Centromere. *Dev. Cell* 6, 253–268. [https://doi.org/10.1016/S1534-5807\(04\)00025-5](https://doi.org/10.1016/S1534-5807(04)00025-5).
69. Xu, Z., Schaedel, L., Portran, D., Aguilar, A., Gaillard, J., Marinkovich, M.P., Théry, M., and Nachury, M.V. (2017). Microtubules acquire resistance from mechanical breakage through intraluminal acetylation. *Science* 356, 328–332. <https://doi.org/10.1126/science.aai8764>.
70. Caballe, A., Wenzel, D.M., Agromayor, M., Alam, S.L., Skalicky, J.J., Kloc, M., Carlton, J.G., Labrador, L., Sundquist, W.I., and Martin-Serrano, J. (2015). ULK3 regulates cytokinetic abscission by phosphorylating ESCRT-III proteins. *eLife* 4, e06547. <https://doi.org/10.7554/eLife.06547>.
71. Chaigne, A., Smith, M.B., Lopez Cavestany, R., Hannezo, E., Chalut, K.J., and Paluch, E.K. (2021). Three-dimensional geometry controls division symmetry in stem cell colonies. *J. Cell Sci.* 134, jcs255018. <https://doi.org/10.1242/jcs.255018>.
72. Cannon, D., Corrigan, A.M., Miermont, A., McDonel, P., and Chubb, J.R. (2015). Multiple cell and population-level interactions with mouse embryonic stem cell heterogeneity. *Development* 142, 2840–2849. <https://doi.org/10.1242/dev.120741>.
73. Mulas, C., Kalkan, T., von Meyenn, F., Leitch, H.G., Nichols, J., and Smith, A. (2019). Defined conditions for propagation and manipulation of mouse embryonic stem cells. *Development* 146, dev173146. <https://doi.org/10.1242/dev.173146>.
74. Kodba, S., and Chaigne, A. (2023). A quick, cheap, and reliable protocol for immunofluorescence of pluripotent and differentiating mouse embryonic stem cells in 2D and 3D colonies. *STAR Protoc.* 4, 102000. <https://doi.org/10.1016/j.xpro.2022.102000>.
75. Schindelin, J., Arganda-Carreras, I., Frise, E., Kaynig, V., Longair, M., Pietzsch, T., Preibisch, S., Rueden, C., Saalfeld, S., Schmid, B., et al. (2012). Fiji: an open-source platform for biological-image analysis. *Nat. Methods* 9, 676–682. <https://doi.org/10.1038/nmeth.2019>.

STAR★METHODS

KEY RESOURCES TABLE

REAGENT or RESOURCE	SOURCE	IDENTIFIER
Antibodies		
alpha Tubulin Monoclonal Antibody	ThermoFischer Scientific	Cat # 62204; RRID:AB_1965960
P-Aurora B Antibody	ThermoFischer Scientific	Cat # PA5-105026; RRID:AB_2816499
Tyrosinated Tubulin	ThermoFischer Scientific	Cat # MA1-80017; RRID:AB_2210201
Aurora B AIM-1	BD Biosciences	Cat # 611082; RRID:AB_2227708
Citron Kinase	BD Biosciences	Cat # 611376; RRID:AB_398898
Acetylated Tubulin	Merck	Cat #T7451; RRID:AB_609894
Acetylated Tubulin	Cell Signaling Technology	Cat #D20G3; RRID:AB_10544694
Donkey anti-Mouse IgG (H + L) Highly Cross-Adsorbed Secondary Antibody, Alexa Fluor™ 488	ThermoFischer Scientific	Cat # A-21202; RRID:AB_141607
Donkey anti-Rabbit IgG (H + L) Highly Cross-Adsorbed Secondary Antibody, Alexa Fluor™ 488	ThermoFischer Scientific	Cat # A-21206; RRID:AB_2335792
Donkey anti-Rat IgG (H + L) Highly Cross-Adsorbed Secondary Antibody, Alexa Fluor™ 647	ThermoFischer Scientific	Cat # A78947; RRID:AB_2910635
Donkey anti-Mouse IgG (H + L) Highly Cross-Adsorbed Secondary Antibody, Alexa Fluor™ 568	ThermoFischer Scientific	Cat # A10037; RRID:AB_11180865
Chemicals, peptides, and recombinant proteins		
RO-3306	Sigma-Aldrich	Cat #SML0569
ZM447439	Selleckchem/BioConnect	Cat #S1103
Barasertib	Selleckchem/BioConnect	Cat #S1147
Okadaic Acid	Alomone lab	Cat #O-800
Taxol	Sigma-Aldrich	Cat # PHL89806
Nocodazole	Sigma-Aldrich	Cat #M1404
UMK57	MedChemExpress	Cat #HY-122236
SiR-tubulin	Spirochrome	Cat #SC002
Deposited data		
All analyzed data	This paper	YODA repository at Utrecht University
Experimental models: Cell lines		
E14 Mouse embryonic stem cells	Niels Geijsen, Hubrecht Institute	N/A
Rex1-GFP Gap43-mCherry	Kevin Chalut, Altos Cambridge	N/A
U2OS stably expressing StableMARK	Lukas Kapitein, Utrecht University	N/A
Software and algorithms		
Fiji/ImageJ	National Institutes of Health, Bethesda, MD, USA	N/A; RRID:SCR_002285
BigTrace	https://github.com/ekatrakha/BigTrace	N/A
UnequalTiffs	https://github.com/ekatrakha/UnequalTiffs	N/A

EXPERIMENTAL MODEL AND STUDY PARTICIPANT DETAILS

E14 Mouse embryonic stem cells (a kind gift from Niels Geijsen, Hubrecht Institute) were used throughout the study. Rex1-GFP Gap43-mCherry (a kind gift from Kevin Chalut, Altos Cambridge) were used for [Video 1](#), and U2OS stably expressing StableMARK⁵⁰ were used for [Figure S3](#). To measure the duration of mitosis in [Figure S1P](#), we used an E14 line stably expressing H2B-RFP.^{71,72}

METHOD DETAILS**Cell culture and transfection****Culture**

E14 Mouse embryonic stem cells were routinely cultured on 10 cm cell culture dishes (Greiner Bio-one, #664160) coated with 0.1% gelatin/PBS in N2B27+2i-LIF with penicillin and streptomycin, at a controlled density ($1.5\text{--}3.0 \times 10^4$ cells/cm 2) and passaged every other day using Accutase (Sigma-Aldrich, #A6964). They were kept in 37°C incubators with 5% CO₂. Cells were regularly tested for mycoplasma. To trigger exit from naive pluripotency, cells were plated in N2B27 after passaging. For a typical experiment, cells were passaged and plated onto laminin for 48h in either N2B27+2i-Lif (naive) or N2B27 (existing). The 2i-Lif media, which sustains naive pluripotency, contains Lif which activates the Jak/STAT pathway, CHIR9902 which promotes Wnt signaling by inhibiting GSK3 β , and the MEK inhibitor PD0325901.⁷³

The culture medium was made in house as described in⁷³ using DMEM/F-12, 1:1 mixture (Sigma-Aldrich, #D6421-6), Neurobasal medium (Life technologies #21103-049), 2.2 mM L-Glutamin (Thermofischer Scientific # 25030024), home-made N2 (see below), B27 (Life technologies #12587010), 3 μ M Chiron (Merck #SML1046), 1 μ M PD 0325901 (Merck #PZ0162), LIF (Merck # ESG1107), 0.1 mM β -Mercapto-ethanol, 12.5 μ g.mL $^{-1}$ Insulin zinc (ThermoFischer Scientific # 12585014). The 200 X home-made N2 was made using 8.791 mg.mL $^{-1}$ Apotransferrin (Sigma-Aldrich #T1147), 1.688 mg.mL $^{-1}$ Putrescine (Sigma-Aldrich #P5780), 3 μ M Sodium Selenite (Sigma-Aldrich #S5261), 2.08 μ g.mL $^{-1}$ Progesterone (Sigma-Aldrich #P8783), 8.8% BSA.

For fixed and live imaging, the cells were plated on 35 mm round Ibidi dishes (IBI Scientific, #81156), coverslips in Invitrogen Attofluor(#A7816) or 8-well Ibidi chambers (IBI Scientific #80807) coated with 10 mg.mL $^{-1}$ Laminin (Sigma #11243217001) overnight at 37°C.

Transfection

For transfection of 3.10^4 cells, a 1 cm 2 well of an 8-well Ibidi chambers (IBI Scientific #80807) coated with 10 mg.mL $^{-1}$ Laminin (Sigma, #11243217001) overnight at 37°C.

1 μ g of DNA was incubated in 50 μ L Optimem (Thermofischer #11058021) for 5 min at room temperature. 1.2 μ L of Lipofectamine (Thermofischer #18324012) was incubated at room temperature in 50 μ L Optimem. The DNA and Lipofectamin solutions were combined and incubated at room temperature for 20 min. Meanwhile, the cells were passaged as described above and seeded in the well from which Laminin has been removed with 100 μ L of culture media (N2B27+2i-Lif for Naive cells or N2B27 for existing cells). The transfection mix was added on top of the cells and the cells were placed in the incubator overnight, and typically rinsed the next morning and imaged in the afternoon.

pTT5 SII-GFP-MCAK (a kind gift from Joyce Meiring, Akhmanova lab) was obtained by cloning cDNAs of the human proteins into pTT5 based expression vectors (Addgene #52355), which also has a Twin-Strep-tag (SII) and a GFP tag.

Drug treatment**Synchronization**

When indicated, cells were synchronized using 10 μ M RO-3306 for 15h and released for 90 min before further treatment. For the time course of bridge maturation, cells were fixed 2h after washing out the RO-3306 which corresponds to bridge formation (0h), or 2h or 4h later.

Inhibition of Aurora-B activity with ZM447439

When indicated, cells were treated with 2 μ M ZM447439 (Selleckchem/BioConnect #S1103) or an equivalent amount of DMSO for 90 min, then rinsed 3 times. For live imaging ZM447439 was not rinsed.

Inhibition of phosphatases PP1 and PP2A and B with Okadaic Acid

When indicated, cells were treated with 0.5 μ M Okadaic Acid (Alomone lab #O-800) or an equivalent amount of DMSO for 60 min, then rinsed 3 times. For live imaging Okadaic Acid was not rinsed.

Inhibition of Aurora-B activity with Barasertib

When indicated, cells were treated with 1 μ M Barasertib (Selleckchem/BioConnect #S1147) or an equivalent amount of DMSO for 90 min, then rinsed 3 times.

Stabilizing microtubules with taxol

When indicated, cells were treated with 0.5 μ M Taxol (Sigma-Aldrich # PHL89806) or an equivalent amount of DMSO for 1h, then fixed. For live imaging cells were treated with 0.5 μ M Taxol at the beginning of imaging.

When indicated, cells were treated with 0.5 μ M Taxol and 2 μ M ZM447439 or an equivalent amount of DMSO for 1h.

Depolymerization of microtubules with nocodazole

When indicated, cells were treated with 0.5 μ M, 1 μ M, 2 μ M, 5 μ M, 10 μ M or 20 μ M Nocodazole or an equivalent amount of DMSO for 1h, then fixed.

MCAK activation with UMK57

When indicated, cells were treated with 2 μ M UMK57 or an equivalent amount of DMSO for 3h30, then fixed.

Immunofluorescence

The primary antibodies used were: alpha Tubulin Monoclonal Antibody (ThermoFischer Scientific #62204), P-Aurora B (ThermoFischer Scientific # PA5-105026), Aurora B AIM-1 (BD Biosciences # 611082), Citron Kinase (BD Biosciences #611376), Acetylated Tubulin (Merck #T7451 and Cell Signaling Technology #D20G3), Tyrosinated Tubulin (ThermoFischer # MA1-80017).

The immunofluorescence was done as described previously.⁷⁴ Briefly, cells were fixed and permeabilised simultaneously using 4% Formaldehyde and 0.1% Triton in PBS for 10 min, rinsed 3 times in PBS then blocked in 3% BSA in PBS for 15 min. Primary antibodies were added at 1:200 in the blocking solution and incubated for 2h at room temperature. Cells were then rinsed 3 times in PBS then blocked for 15 min with the blocking solution and incubated with the secondary antibodies at 1:500 for 1h at room temperature. Cells were then rinsed 3 times with PBS, incubated for 10 min with Hoechst, rinsed 3 times with PBS, and kept in PBS until imaging.

For imaging of fixed samples, a Zeiss LSM 519 700 confocal setup was used. It consists of an AxioObserver Z1 microscope with a Plan-Apochromat 520 63 \times /0.8 oil objective. The set-up was controlled using ZEN.

In figures, a Z-projection over the height of the whole cell is shown. The bridges are shown with the staining of tyrosinated or acetylated tubulin. Bridges are highlighted with pink asterisks.

Live imaging

For live imaging of microtubules, cells were incubated overnight with 20 nM SiR-tubulin (Spirochrome #SC002).

Live imaging was performed using a 60 \times (Plan Apo VC, NA 1.4; Nikon) oil-immersion objective on a Spinning Disc (Yokogawa CSU-X1-A1) Nikon Eclipse Ti microscope with Perfect Focus System equipped with a sample incubator (Tokai-Hit) and an Evolve 512 EMCCD camera (Photometrics), controlled with MetaMorph 7.7 software (Molecular Devices). Cobolt Calypso 491 nm and Cobolt 647 nm lasers were used for excitation. Images were acquired every 5 min.

Colony-forming assay

Colony-forming assays were performed to test the dynamics of exit from naive pluripotency. Cells were plated at low density (3.10^4 cells per well of a 24-well plate) onto plates coated with 0.1% gelatin in N2B27 for 20 h. Cells were resuspended, counted, and plated at clonal density (300 cells per well of a 12-well plate) on 0.1% gelatin in N2B27+2i-LIF. After 5 days, the number of colonies was manually counted.

QUANTIFICATION AND STATISTICAL ANALYSIS

Image analysis

All images were analyzed in Fiji/ImageJ (National Institutes of Health, Bethesda, MD, USA).⁷⁵ Raw images were used for quantification. The contrast was adjusted for clarity of presentation in the figures.

Abscission duration scoring in live cells

Throughout the manuscript, we call abscission the moment where we see rupture of the whole lattice of microtubules in the bridge followed by a recoil of one or both side of the cut bridge. This is in line with our data showing that in ESC membrane rupture directly follow the rupture of the microtubule lattice (Video 1).

Number of bridges

To calculate the ratio between number of cells and number of bridges, the number of bridges was counted using the tubulin channel and the number of cells was counted using a marker of the nucleus (for example Hoechst or Aurora B). The number of bridges was then divided by the number of cells. A higher ratio suggests that abscission is slow.

Bridge length

To measure bridge length, a segmented line was used to trace the microtubules of the bridge from one cell to another cell. This measurement is used as bridge length.

Intensity of Aurora B/P-Aurora B/total tubulin/tyrosinated/acetylated tubulin

To measure intensities in intercellular bridges, a Region Of Interest (ROI) was created surrounding the bridge using one of the tubulin channel and the sum intensity projection was made of the slices in which a bridge was visible. Only flat bridges were selected. The mean Aurora B/P-Aurora B/tubulin intensity was measured using the ROI. To calculate the mean intensity of Aurora B/P-Aurora B/tubulin in the bridge, the background mean intensity was subtracted from the mean intensity of Aurora B/P-Aurora B/tubulin measured in the bridge. All intensities are normalized to the size of bridges.

Intensity of SiR-tubulin and StableMARK

To measure the intensity of SiR-tubulin and StableMARK in intercellular bridges over time, a maximum intensity projection was made of the slices in which a bridge was visible. A bleaching correction was applied to all images. This was done by using the Bleach Correction plugin in Fiji and the chosen correction method was Simple Ratio. The bridge was manually segmented in Fiji using the tubulin channel in every time frame and the SiR-tubulin or StableMARK mean intensity was measured in that area. Only flat bridges were used. To calculate the mean intensity of SiR-tubulin and StableMARK in the bridge, the background mean intensity was subtracted from the mean intensity of SiR-tubulin/StableMARK measured in the bridge.

Kymographs of tubulin intensity at the bridge

To trace the bridges overtime, the BigTrace (<https://github.com/ekatrukha/BigTrace>) plugin was used. The tubulin signal was traced using one click tracing and automated track option. Traced bridges were straightened using the same plugin and respective ROIs were extracted. To concatenate the ROIs, the UnequalTiffs (<https://github.com/ekatrukha/UnequalTiffs>) plugin, which generates a movie of the straightened bridge, was used. The kymographs were generated using KymographBuilder (<https://imagej.net/plugins/kymograph-builder>).

Statistical analysis and data display

Data is given as mean \pm s.d. (standard deviation). Means of two groups were compared by an appropriate test (Student's t-test if the data was normal with a similar standard deviation, with Welch correction if the standard deviation was different, or Mann-Whitney if the distribution was not normal). Anovas were performed in cases with more than 2 groups. In cases where representative intercellular bridge images are shown, similar observations were made in at least 10 bridges from at least 3 independent experiments. Different replicates are shown as variations of the main colors (for example, 3 shades of gray).

Graphs were generated in GraphPad Prism (MathWorks, Natick, MA, USA). Fiji was used to scale images and adjust brightness and contrast. Figures were assembled in Adobe Illustrator (Adobe Systems, Mountain View, CA, USA).